

Heat and Mass Transfer

Nickolai M. Rubtsov

The Modes of Gaseous Combustion

 Springer

Contents

Part I Propagation of Laminar Spherical Flames

1	Flame Propagation: Theoretical Approaches	3
1.1	Influence of Chemically Active Additives on Flame Velocity of Rich $H_2 + Air$ Mixtures	4
1.2	Concentration Limits of Combustion in Rich Hydrogen–Air Mixtures in the Presence of Inhibitors	13
1.3	On the Nature of an Upper Concentration Limit of Flame Propagation in an $H_2 + Air$ Mixture	17
	References.	24
2	Flame Propagation by Spark Discharge Initiation	27
2.1	Influence of Inert Additives on the Time of Formation of Steady Spherical Flame Front of Mixtures of Natural Gas and Isobutylene with Oxygen Under Spark Initiation.	27
2.2	Influence of Inert and Active Additives on the Features of Initiation and Propagation of Laminar Spherical Flames at Atmospheric Pressure.	33
2.3	Numerical Investigation of Effects of Surface Recombination and Initiation for Laminar Hydrogen Flames at Atmospheric Pressure.	40
2.4	Investigation into Regularities of Lean Hydrogen–Air Mixtures Combustion at Atmospheric Pressure by Means of High-Speed Cinematography	44
	References.	52

3	Ignition and Flame Propagation in Heated Vessels	55
3.1	Investigation into Thermal Ignition in Chain Oxidation of Hydrogen, Natural Gas, and Isobutene by Means of High-Speed Color Cinematography	55
3.2	Investigation into Spontaneous Ignition of Propane–Air and n-Pentane–Air Mixtures in Heated Vessel at Atmospheric Pressure by Means of High-Speed Color Cinematography	62
3.3	On the Features of the Negative Temperature Coefficient Phenomenon in Combustion of n-Pentane–Air Mixtures.	68
3.4	Investigation into Spontaneous Ignition of Hydrogen–Air Mixtures in a Heated Reactor at Atmospheric Pressure by Means of High-Speed Color Cinematography.	74
	References.	81
4	Some Features of Kinetic Mechanisms of Gaseous Combustion . . .	83
4.1	Initiation of Hydrogen Flame by a Local Source.	83
4.1.1	Appendix	95
4.2	Various Influences of Active Chemical Additives on Hydrogen and Hydrocarbon Combustion.	97
4.3	Experimental	98
4.4	Results and Discussion	100
4.4.1	Effect of Reactive Additives on the Initiated Ignition of H ₂ and Hydrocarbons in Oxygen.	100
4.4.2	Effect of Small Chemically Active Additives on the Combustion of NG–Air Mixtures at 1 atm	103
4.4.3	Thermal Ignition of Hydrogen and Natural Gas Mixtures with Oxygen in the Presence of Chemically Active Additives	106
	References.	108

Part II Unsteady Gaseous Combustion

5	Instabilities in Gaseous Combustion.	113
5.1	Flame Propagation Regimes at Combustion of Lean Hydrogen–Air Mixtures in the Presence of Additives at Central Spark Initiation at Atmospheric Pressure	115
5.1.1	Experimental	116
5.1.2	Results and Discussion	117
5.1.3	Appendix	125
5.2	Cellular Combustion at the Transition of Spherical Flame Front to Flat Front at Initiated Ignition of Methane–Air, Methane–Oxygen, and n-Pentane–Air Mixtures.	127
5.2.1	Appendix	132

5.3	Establishment of Some Features of Propagation of Unstable Flames by 3D Optical Spectroscopy and Color Speed Cinematography	133
5.4	Acoustic Instabilities in Hydrogen–Air Mixtures in the Closed Reactor at the Central Spark Initiation	140
5.4.1	Experimental	141
5.4.2	Results and Discussion	142
	References.	148
6	Flame Interaction with Obstacles.	151
6.1	Interaction of Spherical Flames of Hydrogen–Air and Methane–Air Mixtures in the Closed Reactor at the Central Spark Initiation with Close-Meshed Obstacles.	152
6.1.1	Experimental	153
6.1.2	Results and Discussion	154
6.2	Interaction of Laminar Flames of Methane–Air Mixtures with Close-Meshed Spherical and Planar Obstacles in a Closed Cylindrical Reactor at Spark Discharge Initiation	159
6.3	Nonsteady Propagation of Single and Counter Flames in Hydrogen–Oxygen and Natural Gas–Oxygen Mixtures in Closed Cylindrical Vessels at Spark Initiation in Initially Motionless Gas.	167
6.4	Penetration of Flames of Methane–Oxygen Mixtures Through Spherical and Planar Obstacles in Closed Cylindrical Reactor	175
6.5	Interaction of Laminar Flames of Natural Gas–Oxygen Mixtures with Planar Obstacles, Diffusers, and Confusers	182
	References.	188
 Part III Critical Phenomena in Supersonic Combustion		
7	Detonation Limits in Gaseous Systems.	193
7.1	Contemporary Approaches to the Description of Processes of Supersonic Combustion	195
7.2	The Influence of an Acoustic Resonator on Flame Propagation Regimes in Spark-Initiated H ₂ Combustion in a Cylindrical Reactor in the Vicinity of the Lower Detonation Limit	205
7.3	Influence of Small Chemical Additives on the Velocity of Detonation Wave and the Detonation Limit in Rich Hydrogen Mixtures	211
7.3.1	Results and Discussion	212
	References.	221

Part IV Role of Disperse Phase in Combustion Processes

8	Phase Formation in Combustion and Pyrolysis	227
8.1	Factors Determining Phase Formation in the Heterogeneous Chain Oxidation of Dichlorosilane at Low Pressures	229
8.1.1	Experimental	231
8.1.2	Results and Discussion	232
8.1.3	Kinetics of Phase Formation	235
8.1.4	SiO ₂ Aerosol Formation in the Presence of CF ₂ Cl ₂ or C ₃ H ₆	236
8.1.5	Model of Phase Formation in a Branching-Chain Process	238
8.1.6	Comparison of Experimental and Calculated Data	243
8.1.7	Appendix 1	246
8.1.8	Appendix 2	248
8.1.9	Three-Dimensional Nucleation	249
8.1.10	Two-Dimensional Nucleation	250
8.1.11	Appendix 3	250
8.2	Formation of Liquid and Solid Dusty Crystals in Gas-Phase Combustion Reactions by the Example of Dichlorosilane Oxidation	251
8.3	Thermal Decomposition of Dichlorosilane: Formation of Threadlike Nanostructures of Silicon and Silicon Carbide by Means of the Method of Chemical Vapor Deposition	257
8.3.1	Experimental	258
8.3.2	Results and Discussion	259
	References	262
9	Features of Combustion of Coal Gas Suspensions	267
9.1	Features of Thermal Ignition of Coal Gas Suspensions, Containing Natural Gas and Oxygen	267
9.1.1	Experiments	268
9.1.2	Results and Discussion	269
9.2	Thermal Ignition of Coal Powders in the Presence of Natural Gas, Oxygen, and Chemically Active Additives	271
9.2.1	Experiments	272
9.2.2	Results and Discussion	273
9.3	Investigation into Ignition of Coal Powders in the Presence of Oxygen and Natural Gas by Means of High-Speed Cinematography	276
9.3.1	Experimental Procedure	277
9.3.2	Results and Discussion	278

9.4	Suppression of Ignition of Coal Powders in the Presence of Oxygen and Natural Gas with Small Additives of Vapor of Octadecafluorodecahydronaphthalene C ₁₀ F ₁₈	283
9.4.1	Experiments	284
9.4.2	Results and Discussion	285
	References.	289
Part V Conclusions		
10	Summary	293



<http://www.springer.com/978-3-319-25932-1>

The Modes of Gaseous Combustion

Rubtsov, N.M.

2016, XXII, 297 p. 127 illus. in color., Hardcover

ISBN: 978-3-319-25932-1

Preface

The book is aimed at the analysis of contemporary problems in combustion science, namely flame propagation, detonation, and heterophaseous combustion based on the works of the author; from a certain viewpoint, it is an auto survey. In this book, some modern problems in the area of gas combustion, as well as methods allowing to calculate and estimate limiting conditions of ignition, and flame propagation on the basis of experimental results obtained substantially by the author of the book are considered. The book may be useful for experienced students and qualified scientists in the area of experimental studies of combustion processes.

An approximate analytical approach for estimation of the effectiveness of the influence of inhibitor additives on flame velocity and flame propagation limits was suggested for combustion of rich H_2 + air mixtures. The method is based on the model of a narrow reaction zone and takes into account peculiarities of the branched chain mechanism of H_2 oxidation. It is shown that the occurrence of flame propagation limits depending on the amount of inhibitor is caused by a positive feedback between flame velocity and the amount of active centers of combustion, being terminated *via* an inhibitor. According to the feedback, the influence of an inhibitor leads to lowering of combustion temperature and flame velocity as well. The method is proposed for the analysis of experimental data on the limits of flame propagation in hydrogen–air mixtures at atmospheric pressure in the presence of small quantities of active additives (inhibitors). The mechanism of the occurrence of an upper concentration limit of flame propagation at atmospheric pressure taking into account effective heat losses in the termolecular recombination $\text{H} + \text{O}_2 + \text{M} \rightarrow \text{HO}_2 + \text{M}$ is suggested for combustion of an H_2 + air mixture.

Regularities of formation of spherical flames in stoichiometric mixtures of natural gas and isobutylene (iso- C_4H_8) with oxygen and Kr or CO_2 additives in the constant volume reactor were established by means of color speed cinematography at 100 Torr and 298 K. The influence of additives of CO_2 , Ar, propene, and CCl_4 on initial stages and dynamics of flame front formation and the structure of laminar spherical flames in hydrogen–air, methane–air, and n-pentane–air mixtures were studied in a bomb of constant volume by means of color high-speed digital

cinematography at atmospheric pressure. Numerical investigation into specific surface effects in flame propagation of lean and rich laminar hydrogen flames at different wall boundary conditions and fuel/air ratios was performed by means of two-dimensional simulations. It was experimentally shown that the same lean ($H_2 < 10\%$) hydrogen–air mixture can be repeatedly ignited. Numerical simulation based on Boussinesq approximation was shown to be in qualitative agreement with the observed features of combustion. Features of spatial development of thermal ignition (so-called self-ignition or spontaneous ignition) in chain oxidation of hydrogen, natural gas, and isobutene with oxygen in the pressure range of 10–100 Torr and 750–1000 K have been revealed by means of high-speed color cinematography. It was shown that the features could be controlled by addition of chemical active gaseous additives (promoters and inhibitors). It is shown that the features of spatial development of spontaneous ignition of propane–air and n-pentane–air mixtures depend on the state of reactor surface, namely an ignition initial center originates on the reactor surface, then the flame front of the center propagates into volume with the normal velocity corresponding to the reactor walls temperature and gas mixture composition. The ignition of n-pentane–air mixture at low temperatures was experimentally studied in a rapid mixture injection static reactor. The ignition process was monitored using a high-speed color video camera. It is shown that introduction of platinum wire into the reactor eliminates the phenomenon of a negative temperature coefficient; however, Pt wire has no effect on the ignition delay time of thermal ignition of stoichiometric n-pentane–air mixture at lower temperatures. Spatial development of chain ignition in hydrogen–air mixtures in the vicinity of the third combustion pressure limit has been investigated by means of quick gas transfer with the use of high-speed color cinematography. It was shown that spatial development of ignition is determined by material and state of the reactor surface; a primary ignition center always occurs at reactor surface.

The approximate analytical method was applied for analysis of the problem on a local chain-thermal explosion in reaction of hydrogen oxidation in the presence of chemically active additive. It is shown that key parameters defining the critical size of a local source of ignition are the temperature in the center of local ignition zone; the quantity of the active centers of combustion created with the local source; and presence of active chemical additives in combustible gas mixture. Comparison to experimental data has shown applicability of the developed approach for the analysis of critical conditions of local ignition in combustible gas mixtures. It is experimentally revealed that the methane combustion inhibitor CCl_4 shows no effect on the lower ignition limit of hydrogen combustion. It is established that small amounts ($\sim 10^{-1}\%$) of chromium hex carbonyl promote combustion of $2H_2 + O_2$ mixture, which manifests itself in the increase in the propagation velocity of the flame, thus inhibition of oxidation of isobutene by this additive takes place. Therefore, the role of hydrogen atoms in hydrocarbon oxidation is not significant and may result at least in participating in longer reaction chains than in hydrogen oxidation. This means that the kinetic mechanism of inhibiting combustion of hydrocarbons by carbonyls suggested in the literature based on accounting for termination of hydrogen atoms should be refined.

By means of high-speed color cinematography, it was shown that the flames in lean H_2 -air mixtures at an initial stage propagate symmetrically and the flame radius can be estimated from the frames of speed filming. It is shown that sufficiently strict calculation of cellular structure of the flame front of lean hydrogen mixtures requires consideration of a 3D problem, however, thermal diffusion instabilities at the initial stage of combustion have no effect on the velocity of flame which can be estimated assuming unperturbed flame front in the range of $8\% < H_2 < 15\%$. It was shown that the analysis of experimental data on flame propagation in lean mixtures does not allow taking apart the results of calculation by two-dimensional model with regard to convection and without convection. It was experimentally shown that isobutene additives in quantities below a concentration limit (up to 1.5%) tend to increase, and CO_2 additives up to 15%—to reduce the flame propagation velocity in lean H_2 -air mixtures. The reasons for the acceleration of combustion in the presence of hydrocarbon additive are considered. The method of high-speed cinematography was used in investigation of transition of spherical flame front to flat front in n-pentane-air and methane-air mixtures initiated by a spark discharge. Cellular flame structures were observed in the transition. Modeling based on compressible reactive Navier-Stokes equations at low Mach number showed qualitative agreement with experiment. Features of combustion in flame cells caused by hydrodynamic instability are experimentally established. It was shown that each flame cell represents a separate “chemical reactor”; in the cell, the process of complete chemical transformation occurs. It was shown that inhomogeneities detected in light emission that arise after contact of a flame front with the walls of cylindrical reactor can be correlated with the occurrence of acoustic waves by the example of combustion of hydrogen-air mixtures containing 30 and 15% of hydrogen. It was revealed that flame velocities in stoichiometric hydrogen-air mixtures at central spark initiation do not depend on the material of inner reactor surface but on its shape.

It was shown that spark initiated flames of hydrogen-air mixtures (8–15% H_2) pass through the close-meshed aluminum spherical obstacles of cell size 0.04–0.1 mm^2 ; the flame of 15% H_2 in the air after obstacle is accelerated; acoustic gas fluctuations occur in the reactor. The flame of 8% natural gas-air mixture is not accelerated after obstacle; acoustic fluctuations are missing. It was shown that active centers of methane and hydrogen combustion, determining flame propagation, have different chemical nature. It was shown that spark initiated flames of diluted stoichiometric natural gas-oxygen mixtures in close-meshed aluminum spheres of mesh size 0.1–0.2 mm^2 do not propagate through the spheres, but always propagate through planar meshed obstacles of the same mesh size. It was found that the features of flame propagation at simultaneous initiation at opposite butt-ends of the cylindrical reactor differ markedly from those at initiation from a single discharge. It is shown that the increase in warming up in hydrocarbons combustion at simultaneous initiation at opposite butt-ends of a cylindrical reactor by a factor of ~ 2 as compared to flame propagation from a single initiation source is due to a two-stage nature of the combustion process. It was shown that ignition of diluted methane-oxygen mix (total pressure up to 200 Torr) after a single obstacle can be

observed markedly far from an obstacle surface. The use of the meshed sphere as an obstacle leads to increase in the distance of flame emergence behind an obstacle in comparison with a round opening; two or more close-meshed obstacles strongly suppress flame propagation. It is experimentally shown that under the same conditions the limit of penetration of diluted methane oxygen flame through a confuser is markedly less than in the case of a plain orifice and is even less than in the case of a diffuser. Therefore, the diffuser is the most effective flame arrester.

It is illustrated that one-dimensional Zeldovich–von Neumann–Doering model of detonation wave gives a satisfactory approach for the description of a stationary detonation wave (DW), despite a large number of the approximations made at the derivation of the equations of the theory. Besides, according to modern literary data on numerical modeling, the neglect of transverse structure of detonation wave in one-dimensional model has no influence on the pressure value in the front of DW in comparison with multidimensional models. It is experimentally demonstrated that the acoustic resonator (Helmholtz's resonator) connected to a cylindrical reactor can cause reactor destruction at spark initiation of deflagration in lean (15 %) hydrogen mixture with oxygen. This points to a possibility of transition of deflagration to supersonic regime mode near the lower concentration limit of detonation even for small reactor where detonation is obviously impossible. On the basis of Zeldovich–von Neumann–Doering detonation theory with allowance for the theory of chain processes by the example of the oxidation of hydrogen-rich mixtures in the presence of chemically active additive (inhibitor), it is shown that taking into account reactions of inhibitor with chain carrier leads to “chemical” losses in addition to heat losses.

A heterophaseous branching-chain reaction of dichlorosilane oxidation is considered in terms of unsteady nucleation theory taking into account the condensation growth of nuclei. The transition between the homogeneous and heterogeneous phase formation; the dependence of the amount of aerosol on the initial temperature, pressure, and mixture concentration; both the kinetics of phase formation and of the disappearance of initial substance are qualitatively described. It is shown that small inhibitor (propene) additives reduce the mean size of aerosol particles. This result is also in qualitative agreement with experimental data. It is found that the amount of aerosol formed decreases with increasing initial temperature because of the increase in equilibrium vapor pressure of the new phase. The reactivity of the silicon dioxide aerosol obtained in the presence of Freon-12 is shown to vary reversibly. The role of surface diffusion and surface nucleation in the deposition of thin films is discussed. We have experimentally observed both the stable liquid and solid Coulomb crystals formed in the discharge-initiated combustion reaction between dichlorosilane and oxygen and the growth dynamics of formation of a rotating solid Coulomb crystal at the interface between the void and dusty cloud. It was shown that the gases evolving during thermal annealing of coal powder have an inhibiting effect on the ignition and combustion of hybrid gas suspension, containing natural gas. Investigation into flammability in oxygen of various types of coal with various content of volatiles at a total pressure of 85 Torr and initial temperatures in the range of 650–750 °C has been performed. It is shown that

ignition of separate particles of coal powder occurs right after injection of powder with oxygen without gas combustion. Then after an ignition delay the volatiles containing in a coal powder ignite, thus the ignition propagates over reactor volume. The more volatiles the coal powder contains the more intensive ignition is observed. It is shown that hybrid powder gas mixture PGM consisting of soot or graphite powders which do not contain volatiles, and a stoichiometric mixture of natural gas and oxygen, intensively ignite in conditions in which hybrid PGM, consisting of coal powder, and a stoichiometric mixture of natural gas and oxygen, does not ignite. It is shown that unlike graphite, soot powder promotes ignition of a stoichiometric mixture of natural gas and oxygen. Possible scenarios of ignitions occurrence in mines were analyzed. It is shown that hybrid PGM, consisting of soot powder and the stoichiometric mixture of natural gas and oxygen, intensively ignites in the absence of $C_{10}F_{18}$, however, in the presence of $C_{10}F_{18}$ combustion of natural gas is missing, the ignition of separate particles of soot powder is only observed.



<http://www.springer.com/978-3-319-25932-1>

The Modes of Gaseous Combustion

Rubtsov, N.M.

2016, XXII, 297 p. 127 illus. in color., Hardcover

ISBN: 978-3-319-25932-1

Chapter 2

Flame Propagation by Spark Discharge Initiation

Abstract Regularities of formation of spherical flames in the mixtures of some hydrocarbons with oxygen and inert additives in the constant volumereactor were established by means of color speed cinematography. Numerical investigation into specific surface effects in flame propagation of lean and rich laminar flames at different wall boundary conditions and fuel–air ratios was performed by means of two dimensional simulations.

Keywords Methane · Isobutene · Hydrogen · Oxidation · Lean · Rich · Two-dimensional simulation · Ignition center · Spherical flame

2.1 Influence of Inert Additives on the Time of Formation of Steady Spherical Flame Front of Mixtures of Natural Gas and Isobutylene with Oxygen Under Spark Initiation

Regularities in the formation of spherical flames in stoichiometric mixtures of natural gas and isobutylene (iso-C₄H₈) with oxygen and Kr or CO₂ additives in the constant volume reactor were established by means of color speed cinematography at 100 Torr and 298 K.

In the majority of combustion processes, chemical reactions in flames have complicated branched-chain nature involving active intermediates (atoms, radicals), therewith the rate of branching strongly depends on temperature [1–4].

Normal velocity of propagation of flame front (FF) U_n accounts for both the chain and thermal accelerating factors of combustion. In the mechanisms of hydrocarbons oxidation, the reaction of nonlinear branching, which can provide a nonthermal flame propagation, is missing [4–6]. Therefore, the only feedback factor responsible for the occurrence of stationary propagating flame is warming-up. Thus, thermal theory [1] with regard to the peculiarities of combustion kinetics [5, 6] is applicable to flame propagation processes.

A zone of FF in the flame of hydrocarbon combustion is comparatively broad. As is known in [2] intensive chain self-acceleration occurs in low-temperature parts of the flames, in this case the nature of the branching step is now under discussion. The peculiarities of the flames on the stage of their origin under spark initiation are scantily known area of combustion physics [1, 2, 4, 7, 8].

The paragraph is aimed at the experimental determination of the conditions of formation of steady spherical FF by means of color speed cinematography of the chemiluminescence of FF. Notice that the zone of intensive chemiluminescence of FF and the zone of maximal change in gas density being recorded by shadow or Schlieren methods do not coincide with each other.

The experiments were carried out under static conditions at 298 K and a total pressure of 100 Torr. A quartz cylindrical reactor (8 cm in diameter, 12 cm height) was equipped with inlets for gas evacuation, spark initiation, and optical windows as well as a pressure transducer. A signal from the pressure transducer was recorded by means of a digital C9-8 oscilloscope and stored in computer memory. Chemiluminescence from FF was recorded by means of color, high-speed, digital camera Casio Exilim F1 Pro (1200 frames/s); each set of frames was stored in computer memory. Ignition was provided with a spark (0.91 J) at the center of the reactor; the distance between the electrodes was 0.05 cm. The reactor was evacuated to 10^{-2} Torr before each experiment. The stoichiometric mixtures of natural gas (NG) and isobutylene (iso-C₄H₈) with CO₂ or Kr additives were prepared prior to experiments. Additives of CO₂ and Kr into the mixture NG + O₂ made up 20–45 % and 30–75 %; and into the mixture iso-C₄H₈ + O₂ made up 35–60 % and 60–80 % correspondingly. NG contained 2 % of propane and butane.

At the initial stage, the flames investigated in the present work appear to be smooth and nearly spherical. Figure 2.1 shows the evolution of captured spherical flames (1200 frames/s, (NG + O₂)_{stoich} + 50 % CO₂, (iso-C₄H₈ + O₂)_{stoich} + 70 % Kr, $P = 100$ Torr, $T_o = 298$ K). A blue, spherical FF due to emission of electronically excited intermediates CH* (431 nm), CH₂O* (470 nm) [2, 11] followed by high-temperature orange area of FF can be easily observed in the frame sets.

It should be noted that the process of formation of the steady FF in H₂–O₂–N₂ and H₂–hydrocarbon–O₂–N₂ flames at 1 atm was investigated in [9]. The results obtained were considered from the only standpoint that the curvature of FF at the initial stage determines the velocity of the rise of origin of initiation. However, as is seen from Fig. 2.2a, b, in which the temporal dynamics of the dependence of the increase in visible radius r_1 of emission of spherical FF on the composition of the mixture is shown, the time of formation of FF increases with decreasing combustibility, i.e., with increasing dilution of a combustible mixture. Moreover, though the local occurrence of secondary hot spots is observed in the mixtures containing NG (Fig. 2.1a), it is seen from Fig. 2.2a that the instabilities do not cause any acceleration of the flame. Notice that in the case of methane–air mixtures no instability effects could be observed [10]. This indicates that combustibility of the mixture along with the curvature of FF determines the time of FF formation.

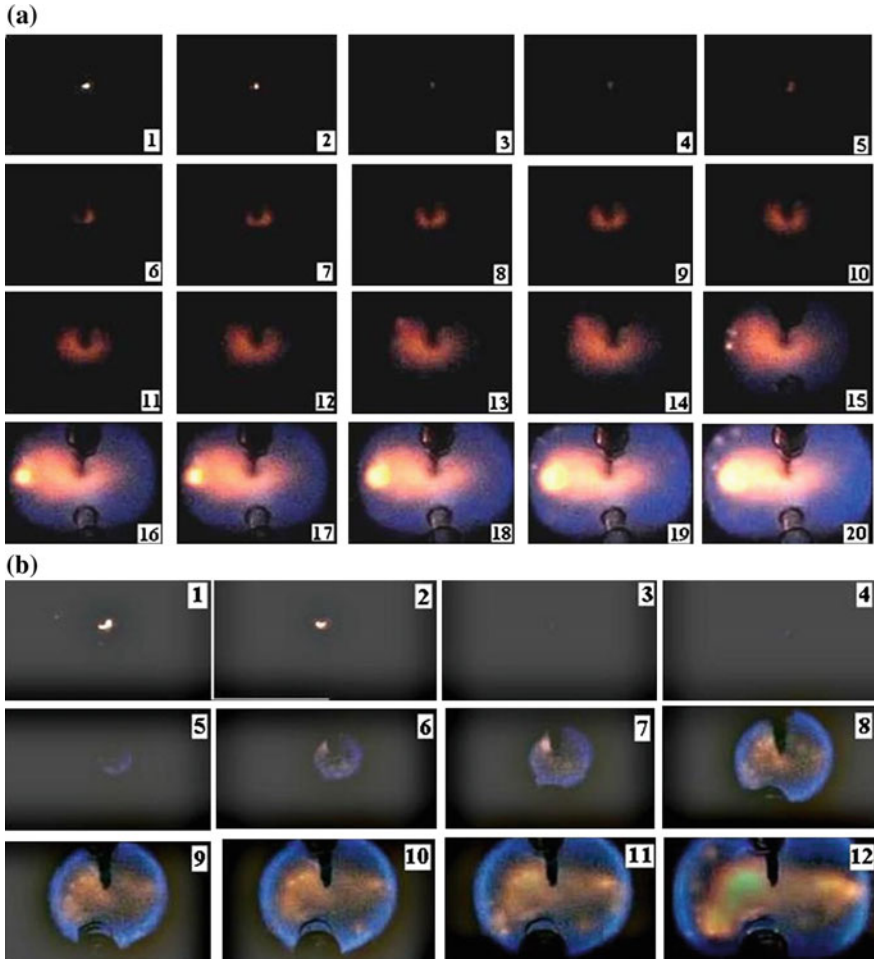


Fig. 2.1 Filming of the propagation of spherical FF (1200 frames/s) **a**— $(\text{NG} + \text{O}_2)_{\text{stoich}} + 50\% \text{CO}_2$, $P = 100 \text{ Torr}$, $T_o = 298 \text{ K}$, $E_o = 0.91 \text{ J}$. **b**— $(\text{iso-C}_4\text{H}_8 + \text{O}_2)_{\text{stoich}} + 70\% \text{ Kr}$, $P = 100 \text{ Torr}$, $T_o = 298 \text{ K}$, $E_o = 0.91 \text{ J}$

Notice that there are no data in the literature on the observation of secondary hot spots in NG combustion detected in this work. The phenomenon needs further investigation.

The data obtained indicate the occurrence of initial hot spot of finite dimension from which the combustion wave can develop. An initial radius of FF for all compositions of gaseous mixtures made up $\sim 0.4 \text{ cm}$. The time of formation of steady FF (τ) was determined from the abscissa of the point of interaction of the line $r = 0.4 \text{ cm}$ and a tangent to experimental dependence $r(t)$. The results of the determination of the values of τ are shown in Fig. 2.3. The data are the evidence for both the occurrence of the hot spot of finite dimension, from which a steady

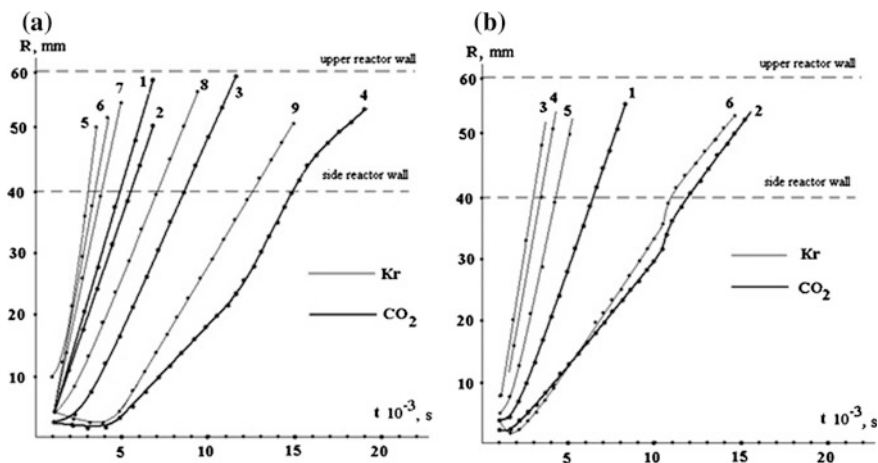


Fig. 2.2 Temporal dynamics of the dependence of the increase in visible radius r_1 of emission of spherical FF on the composition of the mixture ($P = 100$ Torr, 298 K): **a** 1–70 % $(\text{NG} + \text{O}_2)_{\text{stoich}} + 30$ % CO_2 ; 2–65 % $(\text{NG} + \text{O}_2)_{\text{stoich}} + 35$ % CO_2 ; 3–60 % $(\text{NG} + \text{O}_2)_{\text{stoich}} + 40$ % CO_2 ; 4–55 % $(\text{NG} + \text{O}_2)_{\text{stoich}} + 45$ % CO_2 ; 5–55 % $(\text{NG} + \text{O}_2)_{\text{stoich}} + 45$ % Kr; 6–50 % $(\text{NG} + \text{O}_2)_{\text{stoich}} + 50$ % Kr; 7–40 % $(\text{NG} + \text{O}_2)_{\text{stoich}} + 60$ % Kr; 8–30 % $(\text{NG} + \text{O}_2)_{\text{stoich}} + 70$ % Kr; 9–25 % $(\text{NG} + \text{O}_2)_{\text{stoich}} + 75$ % Kr; **b** 1–50 % $(\text{iso-C}_4\text{H}_8 + \text{O}_2)_{\text{stoich}} + 50$ % CO_2 ; 2–40 % $(\text{iso-C}_4\text{H}_8 + \text{O}_2)_{\text{stoich}} + 60$ % CO_2 ; 3–40 % $(\text{iso-C}_4\text{H}_8 + \text{O}_2)_{\text{stoich}} + 60$ % Kr; 4–35 % $(\text{iso-C}_4\text{H}_8 + \text{O}_2)_{\text{stoich}} + 65$ % Kr; 5–30 % $(\text{iso-C}_4\text{H}_8 + \text{O}_2)_{\text{stoich}} + 70$ % Kr; 6–20 % $(\text{iso-C}_4\text{H}_8 + \text{O}_2)_{\text{stoich}} + 80$ % Kr

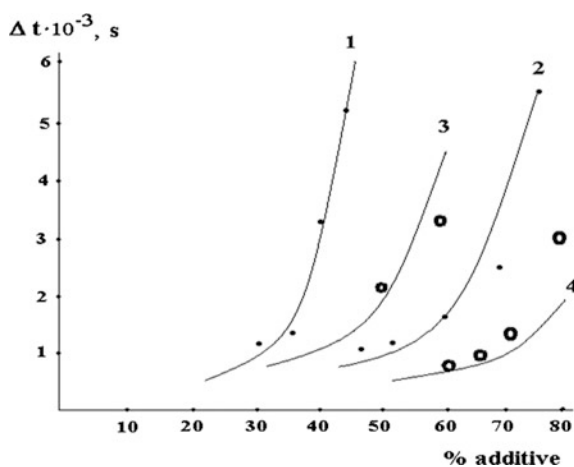


Fig. 2.3 Dependence of the time of formation of steady spherical FF on the composition of a combustible mixture ($P = 100$ Torr, 298 K): 1 $(\text{NG} + \text{O}_2)_{\text{stoich}} + \text{CO}_2$; 2 $(\text{NG} + \text{O}_2)_{\text{stoich}} + \text{Kr}$; 3 $(\text{iso-C}_4\text{H}_8 + \text{O}_2)_{\text{stoich}} + \text{CO}_2$; 4 $(\text{iso-C}_4\text{H}_8 + \text{O}_2)_{\text{stoich}} + \text{Kr}$. Dotted line estimation from Eq. (2.1.8)

combustion wave can develop [12] and of the minimal energy of ignition Q_{MHH} corresponding to this hot spot.

Let us estimate the value of Q_{min} from the data of Fig. 2.2a, b and correlate it with literature values of Q_{min} [9, 12]. We set up a heat balance for the element of the flame with a dimension about the width of steady FF:

$$Q_{\text{MHH}} = V_{\text{min}} \rho C_p (T_b - T_0) \quad (2.1.1)$$

C_p —heat capacity (cal/mol grad), ρ —density of the products in the hot spot (mole/cm³), T_b —temperature of combustion, T_0 —initial temperature, $V_{\text{min}} \sim 4/3 \pi r_{\text{min}}^3$ —minimal volume of the spherical hot spot heated to T_b ; the hot spot will not damp out if its dimension is about the width of the steady FF [12]. In the view of Eq. (2.1.1) and with allowance made for $\rho = (1/N) (P/P_0) (T_0/T_b)$, putting experimental value $T_b \sim 1600$ K, $N = 22.4 \times 10^3$ cm³, $P_0 = 750$ Torr, $T_0 = 298$ K, $P = 100$ Torr, $C_p \sim 10$ cal/mol grad, $r_{\text{min}} \sim 4$ mm we get $Q_{\text{min}}(P) \sim 4.4 \times 10^{-3}$ cal = 1.9×10^{-2} J at 100 Torr for a combustible mixture of (NG + O₂)_{stoich} with the addition of Kr or CO₂. As is known from [12] $Q_{\text{min}}(P_0)$ makes up $\sim 0.33 \times 10^{-3}$ J for methane–air mixture under spark initiation at normal conditions. To compare the values of $Q_{\text{min}}(P)$ и $Q_{\text{min}}(P_0)$ let us estimate the character of dependence of $Q_{\text{min}}(P)$ on pressure. According to [12], minimal dimension of the hot spot makes up $r_{\text{min}} = b\delta$, where b —a nondimensional number ~ 3 , δ —the width of FF, $\delta = \alpha/U_n$, $\alpha = \lambda\rho C_p$ —temperature conductivity, λ —thermal conductivity. Substituting values of r_{min} and δ into Eq. (2.1.1) one can obtain in accordance with [12]:

$$Q_{\text{min}} = 4/3\pi(b\lambda/U_n)^3(P_0/P)^2(N T_b/C_p T_0)^2(T_b - T_0) = \text{const}(1/U_n^3)(P_0/P)^2 \quad (2.1.2)$$

With regard to a weak dependence of U_n on total pressure (U_n slightly changes under change of pressure from 0.1 to 1 atm for methane–air mixtures [5, 8]) the value of Q_{min} from [12] for total pressure makes up 3.3×10^{-2} J. A good agreement between the values obtained by distinct ways is evident in favor of the chosen value of initial radius of FF.

Let us estimate the relationship between values of τ from the data of Fig. 2.3. We consider heat balance at the limit of initiation. The occurrence of the steady hot spot leading to FF propagation is probable under the following condition:

$$q_{\text{min}} \geq q_t \quad (2.1.3)$$

where q_{min} is the rate of heat release in the hot spot, q_t is the rate of heat emission:

$$q_{\text{min}} = V_{\text{min}} Q_0 \omega \quad (2.1.4)$$

$$q_t = \chi S_{\text{min}}(T_b - T_0) \quad (2.1.5)$$

where V_{\min} —volume of the hot spot with radius of r_{\min} , Q_o —heat of combustion of the mole of combustion products, ω —the rate of chemical transformation, χ —heat transfer coefficient, S_{\min} —an area of the surface of the hot spot. With regard to both $r_{\min} \approx \text{const}$ and $Q_o = \text{const}$, the value of q_{\min} can be represented in the form:

$$q_{\min} = Q_{\min}^o / \Delta t \quad (2.1.6)$$

where $Q_{\min}^o \approx Q_{\min}$, and $\Delta t \sim 1/\omega$ —characteristic time of chemical transformation. According to Eqs. (2.1.4)–(2.1.6) we have:

$$Q_{\min}^o / \Delta t \geq \chi S_{\min} (T_b - T_o) \quad (2.1.7)$$

On dilution of the initial stoichiometric mixture with an inert additive the following relation between the times Δt_1 and Δt_2 for different amounts of the same inert additive must assert:

$$\Delta t_2 / \Delta t_1 = (T_{b1} - T_o) / (T_{b2} - T_o) = (\varepsilon_{T1} - 1) / (\varepsilon_{T2} - 1) \quad (2.1.8)$$

where $\varepsilon_T = \nu T_b / T_o$ —a degree of expansion of products of combustion at the given composition of combustible mixture, ν —change in the number of moles in combustion. The value of ν for hydrocarbons under investigation can be put ~ 1 [5], that is $\varepsilon_T \approx T_b / T_o$. The value of ε_T was determined from the value of the end pressure for adiabatic conditions of combustion of combustible mixture P_{bv} [1, 8]: $P_{bv} / P_o = 1 + \gamma(\varepsilon_T - 1)$ where γ is the adiabatic exponent taken equal to 1.2. The value of U_n was determined from the relation $U_n = V / \varepsilon_T$ [5, 8] (V —visible flame velocity).

The values of Δt_1 with respect to one of the experimental values taken as $\Delta t_2 = 0.7 \times 10^{-3}$ s were estimated on the basis of Eq. (2.1.8) with consideration for known values of ε_T . Results of comparison of the experimental values of $\Delta t \sim 1/\omega$ and obtained on the basis of Eq. (2.1.8) are shown in Fig. 2.3 and demonstrate reasonable agreement.

As is seen from Fig. 2.2 CO_2 additives have a more effective influence on the limit of ignition than Kr additives. It can be explained by the fact that CO_2 has greater capacity than Kr, therefore CO_2 additives reduce combustion temperature to a greater extent than Kr and according to Eq. (2.1.8) increase the values of Δt . This causes the breakdown of ignition at lower concentrations of the additive. In addition an increase in Δt may be the result of the greater effectiveness of termolecular chain termination of active centers of combustion in the case of CO_2 as a third body [5].

It was also shown that repeated spark initiation is required in the immediate vicinity of the limit of ignition diluted with CO_2 or Kr combustible mixtures to provide flame propagation. This is the evidence of the important role of low-temperature reactions close to the limit of ignition. It means that a portion of the energy of a spark discharge is consumed to run endothermic reactions of formation of long-lived intermediates (peroxides, aldehydes, etc.), their accumulation provides ignition of the combustible mixture.

Notice that both a solution of a problem on a hot spot thermal explosion and the analysis of unsteady ignition of a hot spot for chemical zero-order reaction are carried out in [13, 14]. In the above examination, authors restricted their consideration to qualitative treatment due to the complicated nature of chemical mechanism of combustion of hydrocarbons.

2.2 Influence of Inert and Active Additives on the Features of Initiation and Propagation of Laminar Spherical Flames at Atmospheric Pressure

The influence of additives of CO_2 , Ar, propylene, and CCl_4 on initial stages and dynamics of flame front formation and the structure of laminar spherical flames in hydrogen–air, methane–air, and n-pentane–air mixtures is studied in a bomb of constant volume by means of color, high-speed, digital cinematography at atmospheric pressure.

Dynamics of formation of a stationary flame front (FF) of a combustible mixture at spark ignition remains a scantily known area of combustion physics [1, 2, 4, 7, 15]. It is due to difficulties of experimental studying of the initial stages of ignition process, namely to short times of FF formation. In Sect. 2.4, see also [15] by means of color, high-speed, digital cinematography the propagation of laminar spherical flames in stoichiometric mixtures of natural gas and isobutylene with oxygen in the presence of Kr and CO_2 was studied in a bomb of constant volume at total pressures up to 100 Torr. It was shown that on dilution of gas mixtures with Kr and CO_2 the time of steady FF formation increases more than by a factor of 10; influence of CO_2 on hydrocarbon combustion is stronger, than that of Kr; the relation of times of FF formation is in inverse proportion to the corresponding relation of warming-ups in these flames.

The present paragraph is aimed at experimental investigation of dynamics of gaseous steady FF formation and its propagation at atmospheric pressure by means of high-speed, color cinematography.

Experiments were performed with stoichiometric methane (CH_4)–air mixtures and n-pentane (C_5H_{12})–air mixtures diluted with inert additives (CO_2 and Ar), at a total atmospheric pressure and initial temperature 298 K. Influence of a chemically active additive on hydrocarbon combustion was investigated by the addition of 2 % CCl_4 to a stoichiometric mixture of 90 % (hydrocarbon–air) + 10.5 % CO_2 . The mixtures 40 % H_2 + 60 % air with 1 ÷ 2 % C_3H_6 additive; 12.5 % H_2 + 87.5 % air and 10 % H_2 + 90 % air without additives were also used in experiments. 1 ÷ 2 % CCl_4 were added to these mixtures for FF visualization. Notice that this amount of CCl_4 does not show any inhibiting action on hydrogen–air combustion [4]. Experiments were performed in a stainless steel reactor of 25 cm in length and 12 cm in diameter, supplied with an optical quartz window of 12 cm in diameter at the butt-end. Spark ignition electrodes were placed in the reactor center. Gas

mixtures were prepared prior to the experiment. The pumped reactor was filled with the gas mixture under investigation to atmospheric pressure; initiation was provided with a spark discharge (0.92 J). Combustion process was recorded by means of a Casio Exilim F1 Pro color, high-speed, digital camera (60–1200 frames/s), sensitive over the spectral range of 420–740 nm. Before each experiment, the reactor was pumped out to 10^{-2} Torr.

The pressure during combustion was recorded by means of a pressure transducer. The dependencies of the radius of a sphere $R(t)$ filled with products of combustion on time were calculated from the initial parts of pressure growth curves [1] obtained in the course of combustion:

$$\frac{R(t)}{R_0} = \left(1 - \frac{(P_b - P(t))(P(t)/P_0)^{-1/\gamma}}{P_b - P_0} \right)^{1/3} \quad (2.2.1)$$

Here R_0 is the reactor radius, P_b is the maximal pressure, P_0 is the initial pressure, $P(t)$ is the current pressure of a gas mixture, γ is the ratio of specific heats (γ was taken equal to 1.2 [1]). From the time dependence of $R(t)$ normal flame velocity $U_n = [dR(t)/dt]/\varepsilon_T$ was calculated. The value of ε_T was determined from the maximal pressure value of combustion P_b [1]:

$$\frac{P_b}{P_0} = 1 + \gamma(\varepsilon_T - 1) \quad (2.2.2)$$

Equations (2.2.1) and (2.2.2) were used for calculation of flame velocities, which were also independently determined from the change of visible radius of a spherical flame.

Typical results of filming of the process of FF formation and propagation are shown in Fig. 2.4 for diluted stoichiometric hydrocarbon–air mixtures. As is seen from Fig. 2.4a, a delay period in the development of the initiation center is observed in combustion of diluted mixture $(\text{CH}_4\text{--air})_{\text{stoich}} + 25\% \text{ Ar}$ (frames 2–9, Fig. 2.4) as well as it was observed in [15] for diluted mixtures at lower pressures.

Dynamics of increase in visible radius of spherical FF for various combustible mixtures was determined from the sequences of images (Fig. 2.5). These results have been independently obtained both by means of image processing of video clips of combustion processes (Fig. 2.5a), and from the initial parts of pressure growth curves obtained in the course of combustion using Eqs. (2.2.1) and (2.2.2) (Fig. 2.5b). From Fig. 2.5 it is possible to determine the time of steady FF formation $-\tau_f$. In Fig. 2.5a it is the moment of the origination of linear dependence of FF coordinate on time and in Fig. 2.5b it is the point of intersection of dependence of FF coordinate on time with x -coordinate. As is seen in Fig. 2.5 the results of measurement of FF velocities with both methods are in good agreement with the literary data, (e.g., the experimental value of U_n in stoichiometric CH_4 –air mixture makes up 30 ± 2 cm/s, and from [15]—35 cm/s). Both the methods independently show that in diluted mixtures constant flame velocity is reached in the certain time interval corresponding to the time τ_f of steady FF formation.

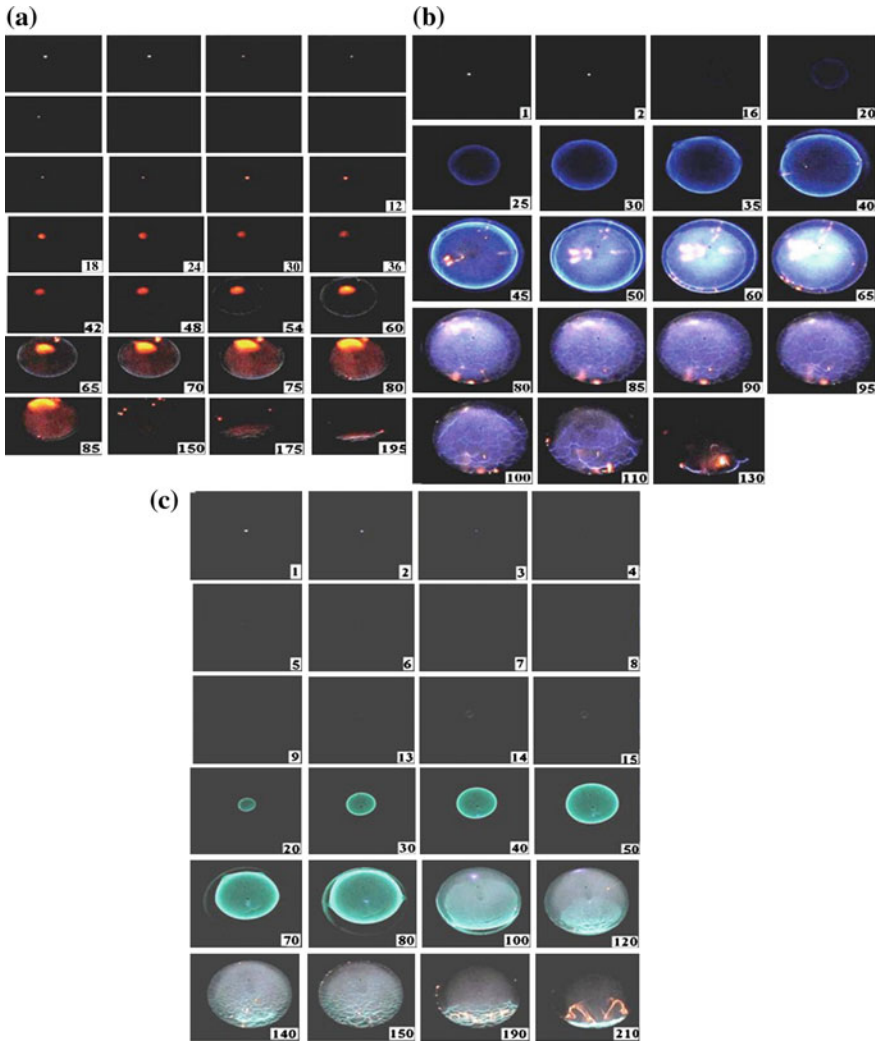


Fig. 2.4 Sequences of video images of propagation of spherical FF. 600 frames/s. Numbers in the picture correspond to consecutive numbers of the video image; **a** $(\text{CH}_4 + \text{air})_{\text{stoich}} + 25\% \text{ Ar}$, $T_0 = 298 \text{ K}$, $E_0 = 0.91 \text{ J}$; **b** $(\text{C}_5\text{H}_{12} + \text{air})_{\text{stoich}} + 10\% \text{ CO}_2$, $T_0 = 298 \text{ K}$, $E_0 = 0.91 \text{ J}$; **c** $(\text{C}_5\text{H}_{12} + \text{air})_{\text{stoich}} + 10\% \text{ CO}_2$, $2\% \text{ CCl}_4$, $T_0 = 298 \text{ K}$, $E_0 = 0.91 \text{ J}$

As is seen from Fig. 2.5 the closer the combustible mixture to a limit of initiated ignition is, the longer τ_f is. Processing of experimental data on the change of visible radius of a spherical flame for the diluted mixtures allowed determining the lower range value of the radius of the initial center of combustion from which the stationary combustion wave [12–14] develops. This radius made up 0.3 cm both for CO_2 and Ar (Fig. 2.5a); CO_2 additives are more effective than those of Ar being in agreement with [15].

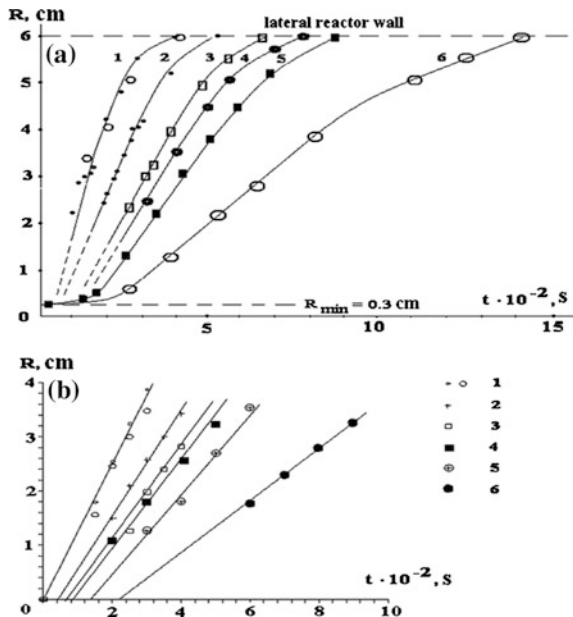


Fig. 2.5 Temporal dynamics of the dependence of the increase in visible radius R of emission of spherical FF on the composition of the mixture (298 K). (1) 90 % $(\text{CH}_4 + \text{air})_{\text{stoich}} + 10$ % Ar, (2) 95 % $(\text{CH}_4 + \text{air})_{\text{stoich}} + 5$ % CO_2 , (3) 80 % $(\text{C}_5\text{H}_{12} + \text{air})_{\text{stoich}} + 20$ % Ar, (4) 90 % $(\text{C}_5\text{H}_{12} + \text{air})_{\text{stoich}} + 10$ % CO_2 , (5) 89.5 % $(\text{C}_5\text{H}_{12} + \text{air})_{\text{stoich}} + 10$ % $\text{CO}_2 + 0.5$ % CCl_4 , (6) 88 % $(\text{C}_5\text{H}_{12} + \text{air})_{\text{stoich}} + 10$ % $\text{CO}_2 + 2$ % CCl_4 . **a** Calculated from the increase in visible radius of front of a laminar flame; **b** calculated from initial sites of pressure growth curves

It was observed that cellular structures arise on FF after the contact of FF with the lateral walls of the reactor (see for example, frame 110 Fig. 2.4b); the average cell size decreases with increase in the concentration of inert diluent (CO_2 or Ar). At flame propagation to butt-ends of the cylindrical reactor cellular structures move in the gravity direction (see Fig. 2.4b, c). As is known [1] cellular flames occurrence is possible in non-stoichiometric flames; the marked difference in diffusivity, for example, of a missing reagent, and thermal diffusivity of combustible mixture is a necessary condition of cellular structure formation. According to the mechanism offered in [1] cellular flame should not occur in stoichiometric mixtures.

This is illustrated in Fig. 2.6, where the result of filming of FF propagation in lean mixture 12.5 % $\text{H}_2 + 87.5$ % air illuminated by 2 % CCl_4 is shown. It is seen from Fig. 2.6a that FF has as a whole a spherical form with the perturbations, whose amplitude increases with increase in the flame radius; the flame radius can be easily estimated from Fig. 2.6a. The normal flame velocity $U_n = V_v/\varepsilon_T$ (V_v —visible flame velocity) determined from Fig. 2.6a from the change of visible radius of a spherical flame using Eqs. (2.2.1) and (2.2.2), makes up 50 cm/s. The normal flame velocity for the mixture 10.0 % $\text{H}_2 + 90.0$ % air makes up 21 cm/s. These values of normal velocity correlate well with literary data [16], and also are close to the results of numerical calculations of U_n obtained by means of a laminar flame model [17, 18]. It means that perturbations observed on FF do not render the essential influence on its velocity at least for $\text{H}_2 > 10$ % in air.

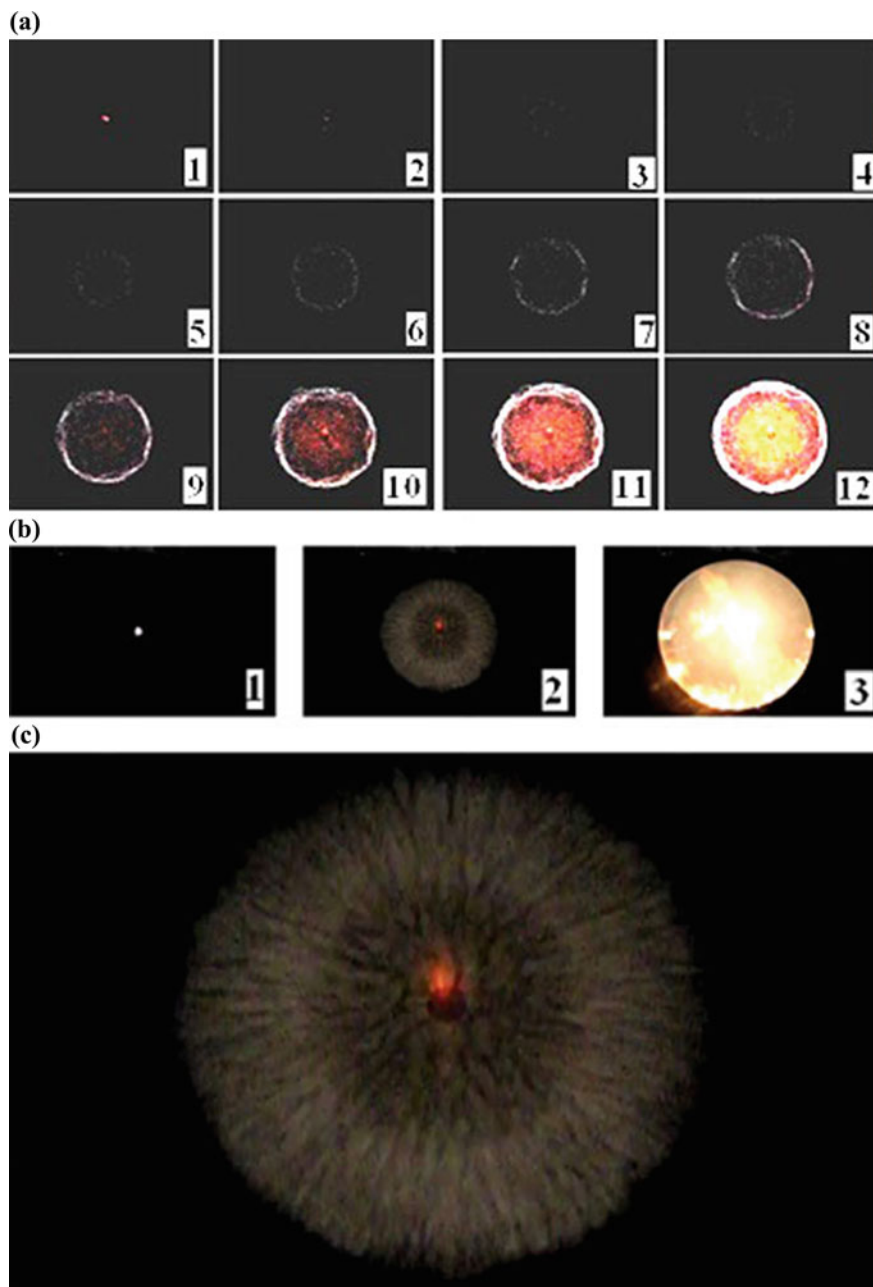


Fig. 2.6 Sequences of video images of propagation of spherical FF illuminated by 2 % CCl_4 , in the mixture 12.5 % H_2 + 87.5 % air. Numbers in the picture correspond to consecutive numbers of the video images. **a** Speed of filming 300 frames/s; **b** Speed of filming 60 frames/s; **c** The enlarged frame 2 of Fig. 2.6b

As is seen in Fig. 2.6b, c it is feasible to register clearly defined cellular structure of FF in the combustion of the mixture 12.5 % H_2 + 87.5 % air at the speed of filming of 60 frames/s due to the long exposition time. It is also seen from Fig. 2.6c (the enlarged frame 2 of Fig. 2.6b) that the front of cellular flame of hydrogen has spherical form and propagates symmetrically from the very beginning of combustion. Therefore, one can assume that the mechanisms of occurrence of cellular flames in combustion of diluted stoichiometric gas mixtures and lean gas mixtures markedly differ.

It has also been shown that in the immediate vicinity of the ignition limit of diluted (with CO_2 or Ar) mixtures repeated initiation by a spark discharge (with an interval ~ 1 – 2 s between discharges) is required for the initiation of flame propagation. It is a possible evidence of the important role of low-temperature reactions at an ignition limit, namely the certain part of spark discharge energy is spent for the formation of long-lived active intermediates (hydroperoxides, aldehydes, etc. [4]). The occurrence of these particles facilitates ignition as they quickly break up or react with formation of chain carriers—free atoms and radicals [4, 7] at higher temperatures in the discharge zone. Such repeated spark initiation provides an increase in temperature in the vicinity of the spark discharge area that should facilitate ignition as well.

To understand the nature of an initial stage of ignition process in the combustible gas mixture it is reasonable to use the results obtained for a problem on the hot spot thermal explosion. The problem on critical conditions of hot spot thermal explosion as well as the analysis of nonstationary ignition of a hot spot for a zero-order chemical reaction is considered in the works [13, 14]. These works will be addressed again at the end of this section. According to [13, 14] the problem on hot spot ignition can be reduced to an examination of the dynamics of a reaction zone on cooling of the hot spot with inert environment. Eventually the cooling of substance on the surface of the hot spot occurs and the border of a reaction zone moves to the center of the hot spot. If by the time when an adiabatic induction period has not yet elapsed the size of a reaction zone is large enough and the heat cannot be removed, the hot spot ignites. Thus, for hot spot ignition it is necessary that during the adiabatic induction period the size of a reaction zone does not become less than a critical size. The sequences of frames shown, for example, in Fig. 2.4a–c, allow considering this model to describe qualitatively hot spot evolution. However, the described model does not take into account the features of the chemical mechanism of process, which can reveal themselves in the strong influence of small chemically active additives on the critical size of a hot spot.

This is demonstrated in Fig. 2.4b–c. The result of high-speed filming of steady FF formation in n-pentane–air mixture in the presence of 10 % CO_2 is shown in Fig. 2.4b. The frame sequences of high-speed filming of FF formation in n-pentane–air mixture in the presence of 10 % CO_2 and 2 % CCl_4 as inhibiting additive is shown in Fig. 2.4c. It is seen that CCl_4 additive provides a marked increase in τ_f and respective reduction of flame velocity.

The considerable influence of the small chemical additive (propene, C_3H_6) on τ_f was also observed for hydrogen combustion. In Fig. 2.7a–d the result of high-speed

filming of steady FF formation in the mixture of 40 % H_2 + 60 % air, illuminated with 2 % CCl_4 in the presence of 1, 1.5, and 2 % of C_3H_6 is shown. We notice that in the same mixture, but without C_3H_6 , FF reaches an upper edge of an optical window by the third frame after spark initiation. It means that the small C_3H_6 additive (1–2 %) provides a marked reduction of flame velocity. It should be noted that the propagation of H_2 –air flame in the presence of 2 % of C_3H_6 is observed only after six consecutive spark initiations of the mixture (Fig. 2.7d). Figure 2.7c corresponds to the third initiation by the spark discharge. It is seen from Fig. 2.7c that the initial center of the combustion was formed, but it did not provide flame propagation.

The data shown in Figs. 2.4 and 2.7 specify that the real evolution pattern of a combustion center of hydrogen and hydrocarbon oxidation in the presence of chemically active additives cannot be well described by the model in which the chemistry of the process is represented by only one reaction in the form of Arrhenius law. This is testified by both strong influence of chemically active additive on the period of steady FF formation and occurrence of critical conditions of initiation. Hence, in the theoretical analysis of a problem on hot spot ignition in gaseous combustion, it is necessary to consider not only cooling the hot spot with inert environment, but also the fluxes of active centers (atoms and radicals) into unreacted gas.

In this paragraph, the quantitative data on times of steady flame front formation in diluted hydrogen and hydrocarbon–air mixtures are obtained. Cellular flames arising in diluted stoichiometric hydrocarbon–air mixtures after the contact of flame front with reactor walls are first observed. The method of color high-speed cinematography allowed establishing that at spark ignition in the vicinity of initiation limit of a gas mixture the initial combustion center of minimum size is formed from which the stationary combustion wave develops.

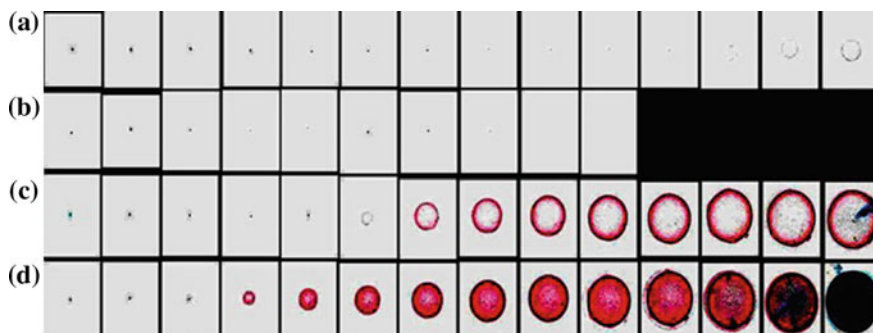


Fig. 2.7 Sequences of video images of propagation of spherical FF in mixture 40 % H_2 + 60 % air in the presence of propylene. The front of a hydrogen flame is illuminated by the addition of 2 % CCl_4 . 1200 frames/s. The colors are inverted. **a** 2 % of propylene, the sixth consecutive initiation by the spark discharge **b** 2 % of propylene, the third consecutive initiation by the spark discharge, **c** 1.5 % of propylene, the first initiation by the spark discharge, **d** 1 % of propylene, the first initiation by the spark discharge

2.3 Numerical Investigation of Effects of Surface Recombination and Initiation for Laminar Hydrogen Flames at Atmospheric Pressure

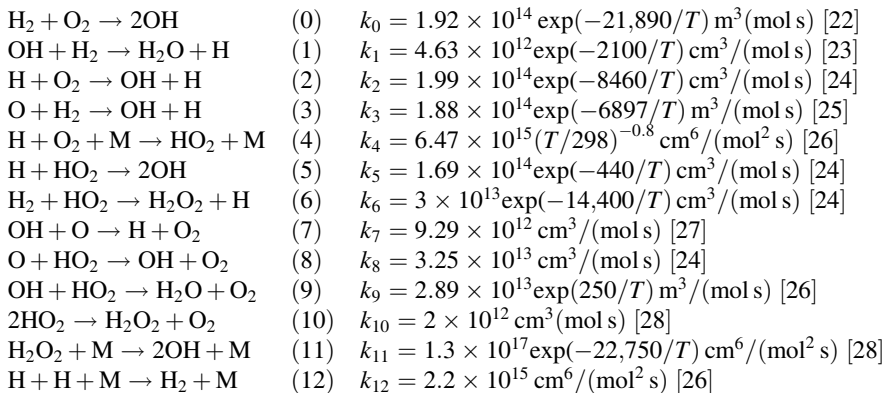
Numerical investigation into specific surface effects in flame propagation of lean and rich laminar hydrogen flames at different wall boundary conditions and fuel/air ratios was performed by means of two-dimensional simulations.

Usage of hydrogen as fuel in engines and other power devices holds the great promise for the decrease of pollution, because the product of the combustion of hydrogen is water. However, the wide application of the fuel is above all retarded with large consumption of energy as well as with the high flammability of hydrogen–air mixtures (HAMs). The combustion of the mixtures often transforms to the detonation regime over a wide range of concentrations of hydrogen. The information on the influence of wall properties on flame propagation in hydrogen–air mixtures is of importance to provide safe conditions of transport and “mobile” storage of hydrogen.

It should be noted that contemporary data on wall effects in hydrogen combustion at 1 atm refer to the conditions of a burner [19, 20]. In these conditions, calculations showed that for the atmospheric pressure of HAM and a wall temperature of 600 K, the catalytic wall retards homogeneous combustion of hydrogen more than the recombination wall.

The paragraph is aimed to numerically investigation of the conditions of steady flame propagation in a tube. The objective was to find the conditions at which surface effects have the influence on the velocities of flame front at atmospheric pressure and wall temperature (300 K) at different wall boundary conditions, reactor diameters, and fuel/air ratios. A surface reaction of chain initiation was also taken into account as well as the specific features of the branched-chain mechanism of hydrogen oxidation.

The reduced kinetic mechanism of hydrogen oxidation at atmospheric pressure can be represented as follows [21]:



As is known, the stationary propagation of a reaction wave must be considered with no regard for a chain origination reaction [1]. Two-dimensional planar problem was examined. Characteristic scales of the process were chosen as follows: $t_0 = 1/(K_1^0[\text{H}_2]_0)$, $x_0 = (D_3/K_1^0[\text{H}_2]_0)^{1/2}$, $U_1^0 = x_0/t_0 = (D_3 K_1^0[\text{H}_2]_0)^{1/2}$ (the scales of time, length, and velocity correspondingly, D_3 is diffusivity of H_2). We determine the dimensionless variables and parameters $\tau = t/t_0$, $\xi = x/x_0$, $\eta = y/y_0$, $\varpi = U/U_0$, $Y_i = [\text{concentration of } i\text{th component}]/[\text{H}_2]_0$, $\delta_i = D_i/D_3$ (D_i —diffusivity of i th component). Velocity and coordinates of the propagating flame front were designated in terms of diffusivity of H_2 (D_3): $\varpi = U/(D_3 K_1^0[\text{H}_2]_0)^{1/2}$, $\xi = x/(D_3/K_1^0[\text{H}_2]_0)^{1/2}$, $\eta = y/(D_3/K_1^0[\text{H}_2]_0)^{1/2}$, here U , x , and y are corresponding dimensional values, K_1^0 —the pre-exponential factor of the reaction (1). Diffusivities (D_i/D_3 , $i = 0-6$) $\delta_0, \delta_1, \delta_2, \delta_3 = 1, \delta_4, \delta_5, \delta_6$ in $\text{H}_2 + \text{air}$ mixture refer to $\text{OH}, \text{O}, \text{H}, \text{H}_2, \text{O}_2, \text{HO}_2, \text{H}_2\text{O}_2$ correspondingly. The set of reaction–diffusion equations for the above reaction mechanism takes the form ($m, n = 0/6$: refer to reacting particles $\text{OH}, \text{O}, \text{H}, \text{H}_2, \text{O}_2, \text{HO}_2, \text{H}_2\text{O}_2$):

$$\begin{aligned} \partial Y_i / \partial \tau &= \delta_i (\partial^2 Y_i / \partial \xi^2 + \partial^2 Y_i / \partial \eta^2) + \sum_{m \neq i, n} k_n Y_m Y_n - \sum_{m=i, n} k_n Y_m Y_n \\ \partial T / \partial \tau &= \delta_7 (\partial^2 T / \partial \xi^2 + \partial^2 T / \partial \eta^2) + 1 / (C_p \rho) \sum_{m, n} Q_n k_n Y_m Y_n \end{aligned} \quad (2.3.1)$$

The rate of heat release in reaction chain is given by the latter equation of the set (2.3.1). Here C_p is the mass-weighted mean specific heat capacity at constant pressure $0.5 \text{ cal g}^{-1} \text{ grad}^{-1}$ for near-stoichiometric mixes [29]; $0.2 \text{ cal g}^{-1} \text{ grad}^{-1}$ for lean mixes, $\delta_7 \approx \delta_3$ is thermal diffusivity of the mixture for near-stoichiometric mixes and $\delta_7 \approx \delta_4$ for lean mixes, T is the temperature (K), ρ is the density of the mixture in g cm^{-3} [29]. Specific heats Q_i and diffusivities were taken from [30, 31]. ϕ is the mole fraction of an initial component.

The reaction–diffusion equation for O atoms as an example is illustrated below:

$$\partial Y_1 / \partial \tau = \delta_1 (\partial^2 Y_1 / \partial \xi^2 + \partial^2 Y_1 / \partial \eta^2) + k_2 Y_2 Y_4 - k_3 Y_1 Y_3 - k_7 Y_0 Y_1 - k_8 Y_1 Y_5$$

The solutions of the set (2.3.1) fulfill the following boundary conditions for the flame propagation from the right to the left (l is the distance between the reactor axis and the reactor wall, symmetry conditions are specified along the axis):

$$\begin{aligned} Y_i(\xi, \eta) &\rightarrow 0 \quad (i \neq 3, 4), \quad T(\xi, \eta) \rightarrow 300 \text{ K}, \quad \xi \rightarrow \pm \infty \\ Y_3(\xi, \eta) &\rightarrow f_{\text{H}_2}, \quad Y_4(\xi, \eta) \rightarrow f_{\text{O}_2}, \quad \xi \rightarrow -\infty; \quad \partial Y_3(\xi, \eta) / \partial \eta \rightarrow 0, \quad \partial Y_4(\xi, \eta) / \partial \eta \rightarrow 0, \quad \eta \rightarrow +\infty \end{aligned} \quad (2.3.2)$$

$$\begin{aligned} Y_i(\xi, l) &= 0, \quad (i \neq 3, 4), \quad \text{or} \quad (\partial Y_i(\xi, \eta) / \partial \eta)_1 = 0; \\ (\partial Y_i(\xi, \eta) / \partial \eta)_1 &= 0, \quad (i = 3, 4); \quad T(\xi, l) = 300 \text{ K} \end{aligned}$$

When solving the set (2.3.1) the initial fronts of the starting components Y_3 [H_2] and Y_4 [O_2] at the time origin over coordinate were defined according to the composition of HAM. The shapes of the fronts were approximated with $\frac{1}{2} - 1/\pi(\arctg(b_i \zeta))$ ($i = 3, 4$), the initial fronts of H atoms and T were specified as $Y_i = a_i \exp(-b_i(\zeta + \eta)^2)$, where a_i and b_i ($i = 2, 7$) were scale coefficients [32]. These initial shapes correspond essentially to the initiation of flame propagation with an external source, as in a number of experiments [4, 16]. The chosen shapes of Y_i had no influence on the steady state values of the velocity of flame propagation. The two-step implicit scheme provided the second order of approximation of the system (2.3.1) over both spatial and time variables [33].

Calculated profiles of chemical components and temperature in a stationary flame front of 40 % H_2 in HAM for the boundary conditions of the types II and I are shown in Fig. 2.8. In Fig. 2.8, the bloom of gray color indicates spatial distributions of concentrations of Y_i , the color borders correspond to fixed concentrations, and a darker color corresponds to greater values of concentrations. As is seen in Fig. 2.8, the profile of OH radicals exhibits two maxima, the result is somewhat similar to the one obtained numerically in [34] for rich HAMs, and it probably has the similar explanation. The top of each frame is the wall of the reactor; the bottom is the axis of the reactor. The use of two types of boundary conditions allowed qualitative establishing the role of surface termination of active centers for different diameters of reactors as well as for different compositions of HAMs. A relation of the velocity for completely inert surface $(\partial Y_i(\zeta, \eta)/\partial \eta)_1 = 0$, $i \neq 3, 4$, II type of boundary conditions) to the velocity for terminating surface $(Y_i(\zeta, 1) = 0$, $i \neq 3, 4$, I type of boundary conditions) was the measure of a wall effect $V_{(\text{flux}=0)}/V_{(\text{conc}=0)}$. The calculations showed (Fig. 2.8c) that the mechanism accepted is valid enough due to the fact that calculated flame velocities for the terminating surface are in good qualitative agreement with the literary data [4].

Calculated dependencies of the values of $V_{(\text{flux}=0)}/V_{(\text{conc}=0)}$ both on H_2 concentration in HAMs and reactor diameter are shown in Fig. 2.9a. As is seen, the influence of wall chain termination at 1 atm increases with decreasing both diameter and H_2 concentration. Figure 2.9b shows that the calculated lower concentration limit makes up about 5 % H_2 ; it is in agreement with literary data [4, 16] and also suggests validity of the mechanism accepted. It is seen from Fig. 2.9b that the influence of surface is most pronounced only in the immediate vicinity of the lower concentration limit; its dependence on the content of H_2 is rather sharp. Therefore, even a flame arrester composed of pipes of 1 cm in diameter treated with the substance, which effectively terminates reaction chains (e.g., metal oxide [35]), will not be efficient if the content of H_2 in HAM exceeds 6 %. The narrower tubes will maintain stronger resistance to the gas flow. It means that the use of small active chemical additives (inhibitors) to prevent explosions of HAMs is considerably more promising [3].

The influence of the rate of surface chain initiation on the velocity of flame propagation was also investigated. It was expected that the surface evolves H atoms; their flux into reactor volume was assumed to make up $\partial Y_2(\zeta, \eta)/\partial \eta)_1 = k_0 Y_1 Y_2 / k_1^0$.

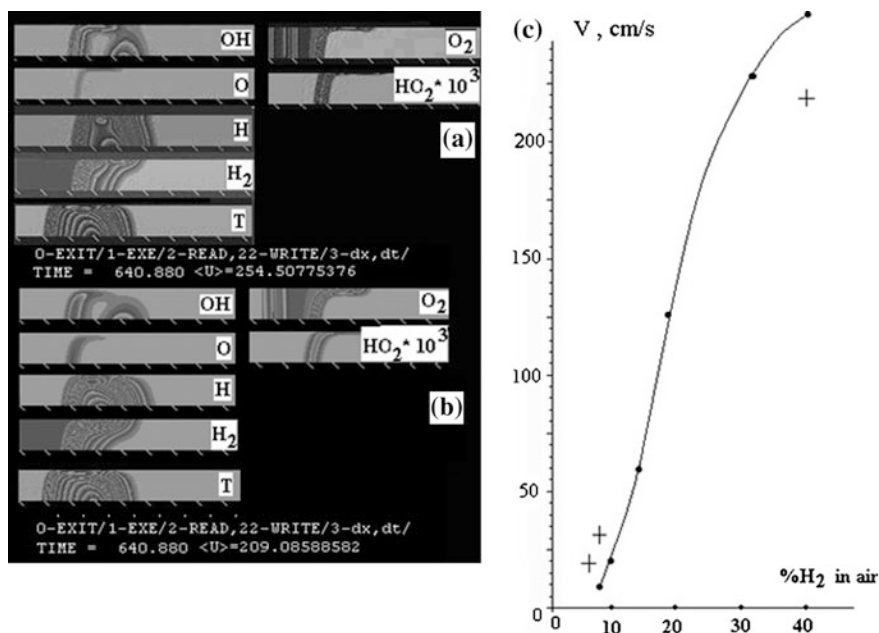


Fig. 2.8 Calculated profiles of chemical components and temperature in a stationary flame front of hydrogen (40 %)-air mixture for I and II types of boundary conditions ($d = 1$ cm). The *top* of each frame is the wall of the reactor; the *bottom* is the axis of the reactor. The flame front moves from the *right to the left*. $P = 1$ atm, wall temperature is 300 K. **a** Fluxes of H, O atoms and OH, HO₂ radicals at the wall are equal to zero. **b** Concentrations of H, O atoms and OH, HO₂ radicals at the wall are equal to zero. **c** Laminar burning velocity of hydrogen–air mixtures at room temperature and atmospheric pressure (circles [19, 20]), calculated in this work for I type of boundary conditions (crosses)

Calculations showed that chain initiation for the mixture of 40 % H₂ in HAM takes effect only if the rate constant of surface initiation amounts to the value of homogeneous initiation k_0 taken at 1800 K; in other words to accelerate flame propagation the surface must exhibit catalytic properties.

It was speculated in [36] that chain branching does not occur in H₂ oxidation at 1 atm. It was of interest to verify whether fast chain initiation could provide stationary flame propagation in the absence of chain branching at given rate constants. For this purpose, it was assumed that the number of free valences does not change in the branching step (2), i.e., the reactions of O atoms formed in step (2) were not taken into consideration in further calculations. Under this assumption, only a trivial solution of the set (2.3.1) was attained. It means that for the accepted chemical mechanism the rate of heat release is not enough to sustain a combustion wave if chain branching does not occur. A wave solution does not exist even at the value of the rate constant of surface initiation k_0 , which influences on flame velocity if the chain branching is taken into account (see above). Therefore, the performed

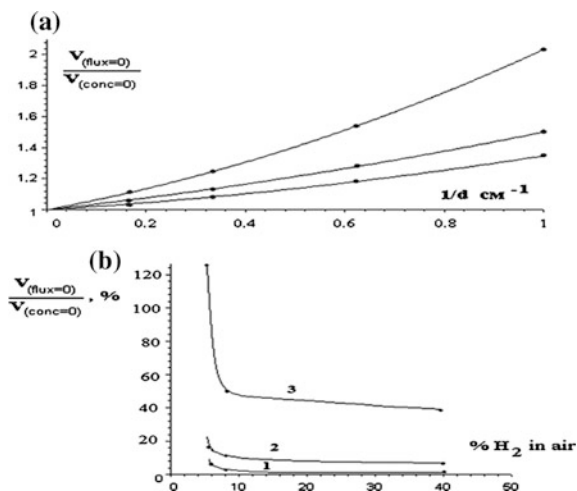


Fig. 2.9 **a** Calculated dependencies of the relation of the velocity for completely inert surface $V_{(flux=0)}$ to the velocity for terminating surface $V_{(conc=0)}$ both on H₂ concentration in mixtures and reactor diameter (*curves are fitted, top-down 6 % H₂, 8 % H₂, 40 % H₂ in air*); **b** Calculated dependencies of the percent of the contribution of surface termination on the concentration of H₂ in air from a plot (a) for three diameters (1, 2, 3) of the reactor (*curves are fitted; vertical line designates the lower concentration limit*); 1–10 cm, 2–5 cm, 3–1 cm

calculations point to the importance of inclusion of the chain branching step for a description of the features of hydrogen combustion at higher pressures [4].

By this means, it has been shown that the influence of surface chain termination on the flame velocity becomes significant in the vicinity of the lower concentration limit; the surface chain initiation does not affect the flame velocity. It has been also shown that the flame propagation does not occur if a chain mechanism without branching even with high rates of chain initiation is used.

2.4 Investigation into Regularities of Lean Hydrogen–Air Mixtures Combustion at Atmospheric Pressure by Means of High-Speed Cinematography

It was experimentally shown that the same lean ($H_2 < 10\%$) hydrogen–air mixture can be repeatedly ignited. Numerical simulation based on Boussinesq approximation is in qualitative agreement with the observed features of combustion.

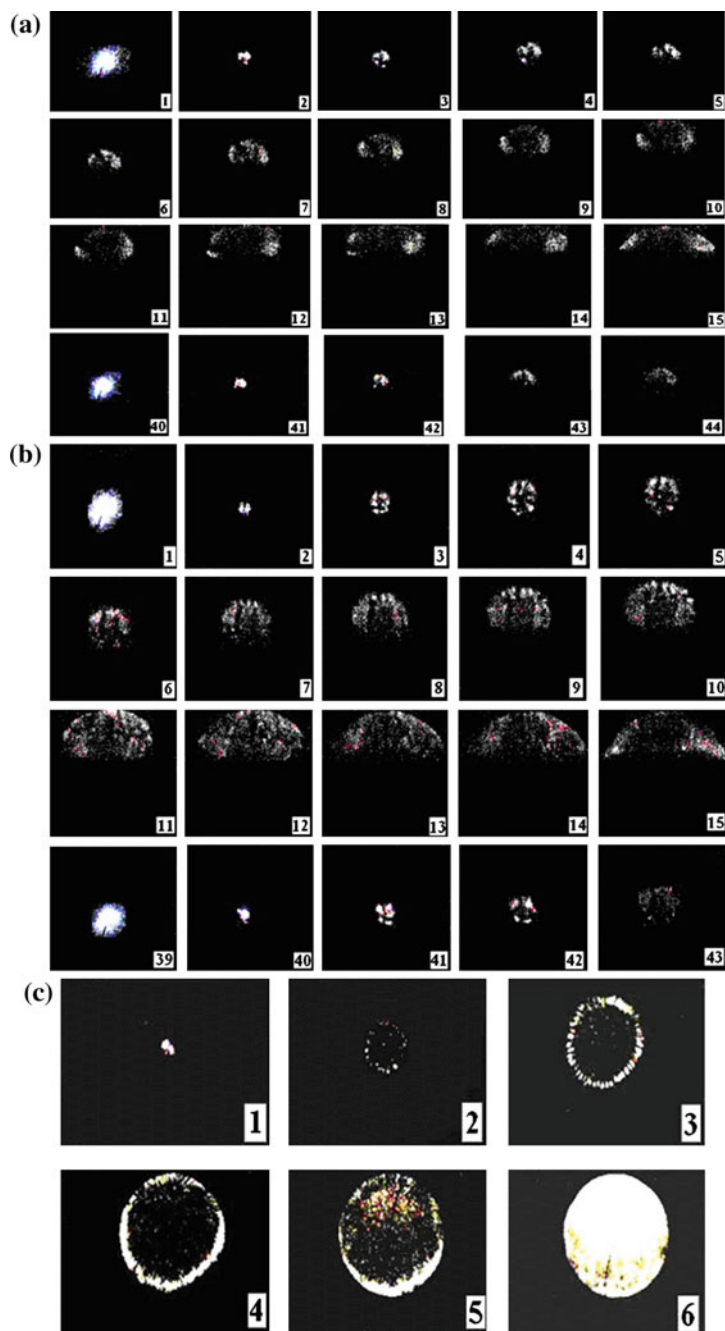
Usage of hydrogen as fuel is terminated with high flammability of its mixtures with air. In this connection, combustion of lean H₂–air mixtures in the vicinity of the lower concentration flame propagation limit (CFPL) is of particular interest. In the mixtures, the flame front (FF) is nonuniform due to the high H₂ diffusivity. It leads to the occurrence of cellular flames [1, 37–39] even if the gravity is missing

[40]. It is shown in [3] that in an upward direction of flame propagation CFPL in lean mixture is lower than in a downward direction; H_2 consumption is incomplete. It is of interest to establish concentration areas of lean mixtures, in which either thermo-diffusive instability or hydrodynamic instability of FF under gravity is the controlling factor. In this work, the method of high-speed, color cinematography was used for these purposes. The method, as distinct from Schlieren cinematography [40], by which only an area of a drastic change of gas density in FF is recorded, is more sensitive because FF emission intensity is determined by the occurrence of nonequilibrium concentrations of active intermediates in flame.

As is known, numerical analysis of the system of three-dimensional balance equations for mass, momentum, and thermal energy for compressible medium along with chemical kinetics equations not always provides a single-valued description of gaseous combustion, and depends on the choice of the model of turbulent flow [39]. Due to aforesaid the present paragraph is aimed at both experimental establishment of the features of initiated ignition of lean H_2 –air mixtures at 1 atm by means of high-speed, color cinematography and numerical simulation of the process under the Boussinesq approximation to describe natural convection [41, 42].

Experiments were performed with mixtures of 4 % CCl_4 + 7.5 % H_2 + 88.5 % air, 4 % CCl_4 + 8 % H_2 + 88 % air, and 4 % CCl_4 + 11 % H_2 + 85 % air. 4 % of carbon tetrachloride (CCl_4) was added for visualization of FF. Notice that the even 5 % CCl_4 additive to lean H_2 –air mixtures does not show any inhibiting action on combustion [4]. Horizontal stainless steel reactor of 25 cm in length and 12 cm in diameter, supplied with demountable covers and an optical window of 10 cm in diameter at a butt-end was used in the experiments [6]. Electrodes of spark ignition were mounted in the reactor center. The gas mixture was prepared in the reactor. First CCl_4 vapor then H_2 and air was allowed to bleed into the reactor to 1 atm. Spark initiation was carried out in 20 min. Ignition and FF propagation were recorded by means of color, high-speed, full HD camera Casio Exilim F1 Pro with a speed 60 frames/s. Before each experiment, the reactor was pumped to 10^{-2} Torr.

The results of filming of FF propagation for mixtures of 4 % CCl_4 + 7.5 % H_2 + 88.5 % air, 4 % CCl_4 + 8 % H_2 + 88 % air, and 4 % CCl_4 + 11 % H_2 + 85 % air at $T = 298$ K and spark energy of $E_0 = 1.5$ J are shown in Fig. 2.10a–c. As is seen in Fig. 2.10 combustion cells are well visualized. In combustion of mixtures (7.5 % and 8 % H_2 in air) movement of FF to the top part of the reactor (Fig. 2.10a, b) was observed. It was shown that after the flame was observed to quench itself after propagating the second flame propagation in the mixture could be initiated once again at the same place by the spark of the same energy (frame 40 Fig. 2.10a and frame 39 Fig. 2.10b). We observed three successive ignitions of the same mixture. As follows from the calculations below, the reactor volume specifies the number of ignitions: with an increase in the volume, the number of repeated ignitions is bound to increase. At the repeated initiation, quantity of cells and FF velocity is approximately the same as at the first ignition. The result obtained indicates the necessity to account for possibility of repeated ignition in lean H_2 –air mixtures under the development of fire control systems. It was also established that



◀ **Fig. 2.10** Sequences of video images of propagation of cellular FF. 60 frames/s. Numbers in the picture correspond to consecutive numbers of the video images. **a** 4 % CCl₄ + 7.5 % H₂ + 88.5 % air, 4 % CCl₄ + 8 % H₂ + 88 % air and 4 % CCl₄ + 11 % H₂ + 85 % air, $T_0 = 298$ K, $E_0 = 1.5$ J. **b** 4 % CCl₄ + 8 % H₂ + 88 % air, $T_0 = 298$ K, $E_0 = 1.5$ J. **c** 4 % CCl₄ + 11 % H₂ + 85 % air, $T_0 = 298$ K, $E_0 = 1.5$ J

in the richest mixture (11 % H₂ + 89 % air) cellular FF extends in all directions practically with the same velocity (Fig. 2.10c), and by a factor of 4 faster, than in the mixtures containing 7.5 and 8 % H₂ in air (Fig. 2.10a, b). This result suggests that at concentration of H₂ more than 10 % flame velocity increases, so that natural convection does not influence on the FF velocity in upward direction. It should be noted that in such mixtures burning “symmetrically”, repeated FF propagation is not observed.

At numerical simulation, we considered a flat two-dimensional system of equations where the reaction–diffusion system is coupled with the Navier–Stokes equations under the Boussinesq approximation to describe the natural convection, which can occur because of the heat produced by the reaction [41, 42]. In this model, changes in density ρ are caused by changes in temperature T (ρ_0 —initial density, β —factor of volume expansion of the medium):

$$\rho = \rho_0 + \delta\rho, \quad \delta\rho \ll \rho_0, \quad \delta\rho = -\rho_0 \cdot \beta \cdot T \quad (2.4.1)$$

Density change is considered only in the equations of movement and is ignored in the continuity equation. Then (after subtraction of hydrostatic pressure $p_0 = \rho_0 g h$) two-dimensional equations of movement and continuity in dimensionless variables are $\xi = x/L_0$, $\zeta = y/L_0$, $\tau = t/t_0$, $\vartheta = u/V_0$, $v = v/V_0$, $\theta = (T - T_0)/(T_c - T_0)$, $\pi = p/P_0$, $Y_i = C_i/[H_2]_0$ where L_0 , t_0 , V_0 , T_0 , P_0 are characteristic dimensional scales of length, time, speed, temperature, and pressure. C_i —concentration of components, $g = 980$ cm/s, u , v —components of current velocity; T_c —adiabatic combustion temperature of the mixture of given composition, T_0 —initial temperature take the form:

$$Re \left(\frac{\partial \bar{V}}{\partial \tau} + \vartheta \frac{\partial \bar{V}}{\partial \xi} + v \frac{\partial \bar{V}}{\partial \zeta} \right) = -\bar{\nabla} \pi + e_y Ra \theta + \Delta \bar{V} \quad \bar{\nabla} \cdot \bar{V} = 0 \quad (2.4.2)$$

where $\bar{V} = V(u, v)$ medium velocity, e_y —unit vector in upward direction. Temperature distribution in gas is described by the heat conductivity equation (χ —thermal diffusivity, Q_i —heat emission sources)

$$\frac{\partial \theta}{\partial \tau} + \vartheta \frac{\partial \theta}{\partial \xi} + v \frac{\partial \theta}{\partial \zeta} = \frac{1}{Pe_T} \Delta \theta + \sum Q_i \quad (2.4.3)$$

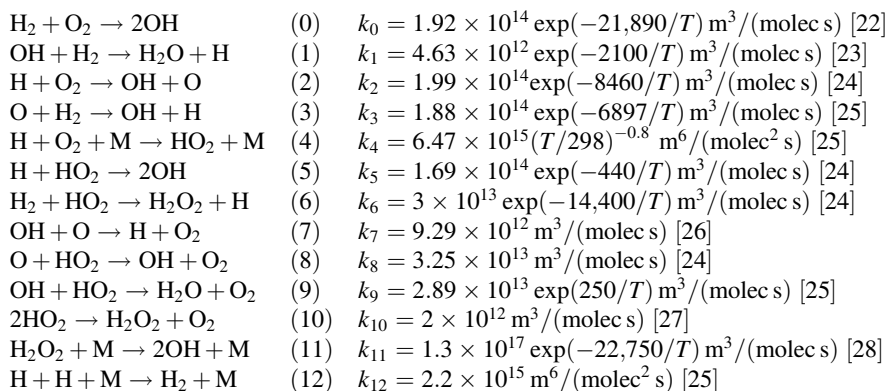
Distributions of component concentration are described by the corresponding reaction–diffusion equations (D_i —diffusivities, K_{ij} —rate constants)

$$\frac{\partial Y_i}{\partial \tau} + v \frac{\partial Y_i}{\partial \xi} + v \frac{\partial Y_i}{\partial \zeta} = \frac{1}{Pe_i} \Delta Y_i + \sum_{ij} K_{ij} Y_i \quad (2.4.4)$$

In Eqs. (2.4.2)–(2.4.4) traditional notations for dimensionless numbers of Rayleigh— Ra , Reynolds— Re and Pecle— Pe_T , Pe_i were used.

$$Ra = \frac{\rho_0 g \beta T_0 L_0^3}{\eta \chi} \quad Re = \frac{\rho_0 L_0 V_0}{\eta} \quad Pe_T = \frac{L_0 V_0}{\chi} \quad Pe_i = \frac{L_0 V_0}{D_i} \quad (2.4.5)$$

Calculations were performed in Cartesian coordinates using uniform grid (513×513 nodes). The second order of approximation of finite difference derivatives was used. Integration of Eq. (2.4.2) was performed in two stages [43]. At first, the movement equations were integrated without pressure forces, and intermediate field of velocities is obtained, then from continuity condition a potential additive to the intermediate field of velocities, corresponding to the action of pressure gradient was calculated. Pressure field was calculated by solving a boundary problem with the use of multigrid techniques [44] for Eq. (2.4.2) which turns out from the continuity condition as a result of substitution of the intermediate field of speeds [33]. After the calculation of the field of speeds, numerical integration of Eqs. (2.4.3) and (2.4.4) is performed to calculate new values of temperature and concentration. On lateral borders of the calculated area, normal derivatives were put equal to zero (a condition of mirror symmetry). Integration of Eqs. (2.4.3) and (2.4.4) was carried out by the modified alternately triangular method [45]. The objective consisted in establishing of possibility of qualitative modeling of both cellular combustion regime and increase in cell quantity with increase of H_2 content as well as repeated initiation of a cellular flame in the mixture, which already burnt. The reduced kinetic mechanism of H_2 combustion at 1 atm was represented in the form [17]:



Dimensionless time scales, lengths, and speeds of process were chosen as follows: $t_0 = 1/(K_1^0 [\text{H}_2]_0)$, $x_0 = y_0 = (D_3/K_1^0 [\text{H}_2]_0)^{1/2}$, $V_0 = x_0/t_0 = (D_3 K_1^0 [\text{H}_2]_0)^{1/2}$, $\delta_4 = \chi/D_3$, где $K_1^0 = 4.63 \times 10^{12}$ is the pre-exponential factor of the reaction (1), D_3 – H_2 diffusivity. Dimensionless variables and parameters took the form $\tau = t/t_0$, $\xi = x/x_0$, $\zeta = y/y_0$, $Y_i = [\text{concentration of } i\text{th component}]/[\text{H}_2]_0$. K_p is dimensionless reaction velocity. For bimolecular step, $K_p = k_p/K_1^0$ p corresponds to the step number ($p \neq 4, 12$). For termolecular step, $K_p = k_p [\text{H}_2]_0/K_1^0$ where $p = 4, 12$. Nondimensional diffusivities $\delta_0, \delta_1, \delta_2, \delta_3, \delta_5, \delta_6, \delta_7$ ($\delta_i = D_i/D_3$, $i = 0-6$) in H_2 –air mixture correspond accordingly to OH, O, H, H_2 , O_2 , HO_2 , H_2O_2 . For example, the heat conductivity equation in dimensionless variables takes the form:

$$\partial\theta/\partial\tau + \partial\partial\theta/\partial\xi + \nu\partial\theta/\partial\zeta = \delta_4(\partial^2\theta/\partial\xi^2 + \partial^2\theta/\partial\zeta^2) + [\text{H}_2]_0/(C_p\rho(T_c - T_0)) \sum_p \sum_{m,n} Q_p K_p Y_m Y_n$$

Here C_p is the average thermal capacity at constant pressure $0.25 \text{ cal g}^{-1} \text{ grad}^{-1}$ [29]; δ_4 is nondimensional thermal diffusivity of the mixture, it is considered that $\delta_4 \approx \delta_5$, ρ —gas density g cm^{-3} , $M = 760 \times 10^{19}/T$, T —temperature (K). Thermal effects of elementary steps Q_i and diffusivities were taken from Refs. [30, 31]. Indexes m, n , which change from 0 to 6, correspond to nondimensional concentrations OH, O, H, H_2 , O_2 , HO_2 , H_2O_2 . The index p at dimensionless rate constants $K_p = k_p/K_1^0$ changes from 0 to 12, and the value of the index corresponds to the reaction number in the kinetic mechanism above. The initiation center was given by an ellipse with axes of 20×30 nodes (Fig. 2.11a, b) in which nondimensional H atom concentration and θ were set equal to $0.4 \div 0.6$. In the calculated area outside of the center of ignition the concentrations of all intermediates were set equal to zero, $\theta = 0$, concentration of H_2 was set equal 6 % и 8 % in air, containing 21 % O_2 . Thus, the solution of the system of Eqs. (2.4.2)–(2.4.4) satisfies to the following initial conditions outside of initiation area: $0 < \xi < L$, $0 < \zeta < L$: $Y_i(0, \xi, \zeta) = 0$ ($i \neq 3, 4$), $Y_3(0, \xi, \zeta) = f_{\text{H}_2}$, $Y_4(0, \xi, \zeta) = f_{\text{O}_2}$; $T(0, \xi, \zeta) = 300 \text{ K}$. Boundary conditions are: $0 < \xi < L$: $T(\tau, \xi, 0) = 300 \text{ K}$, $T(\tau, \xi, L) = 300 \text{ K}$, $0 < \zeta < L$: $T(\tau, 0, \zeta) = 300 \text{ K}$, $T(\tau, L, \zeta) = 300 \text{ K}$. On the boundaries, the termination of active centers is missing:

$(\partial Y_i(\tau, \xi, \zeta)/\partial\zeta)_L = 0$ ($\partial Y_i(\tau, \xi, \zeta)/\partial\xi)_L = 0$ where L is dimensionless length and width of the channel, corresponding to dimensional size of 5.9 cm under our conditions, f_{H_2} , f_{O_2} —fractions of initial reagents $[\text{H}_2]_0$ and $[\text{O}_2]_0$ in the mixture.

Calculated profiles of H atoms in FF for $[\text{H}_2]_0 = 6 \%$ and $[\text{H}_2]_0 = 8 \%$ are shown in Fig. 2.11a, b, respectively. The shade of gray color in Fig. 2.11 defines the value of H atom concentration, more light color corresponds to the larger values of concentration. We will notice that the best agreement with experimental data presented in Fig. 2.10 is reached at $[\text{H}_2]_0 = 4 \%$ and $[\text{H}_2]_0 = 6 \%$, respectively. It should be noted that for the kinetic scheme above the value of lower CFPL at 1 atm is equal to 2 %. The value is in qualitative agreement with [38] where is shown that in an upward direction of flame propagation CFPL is lower than in a downward direction. It is known, however, [46] that the value of CFPL can even reach 3 %, depending on both spark power and the recording procedure. Notice that the model

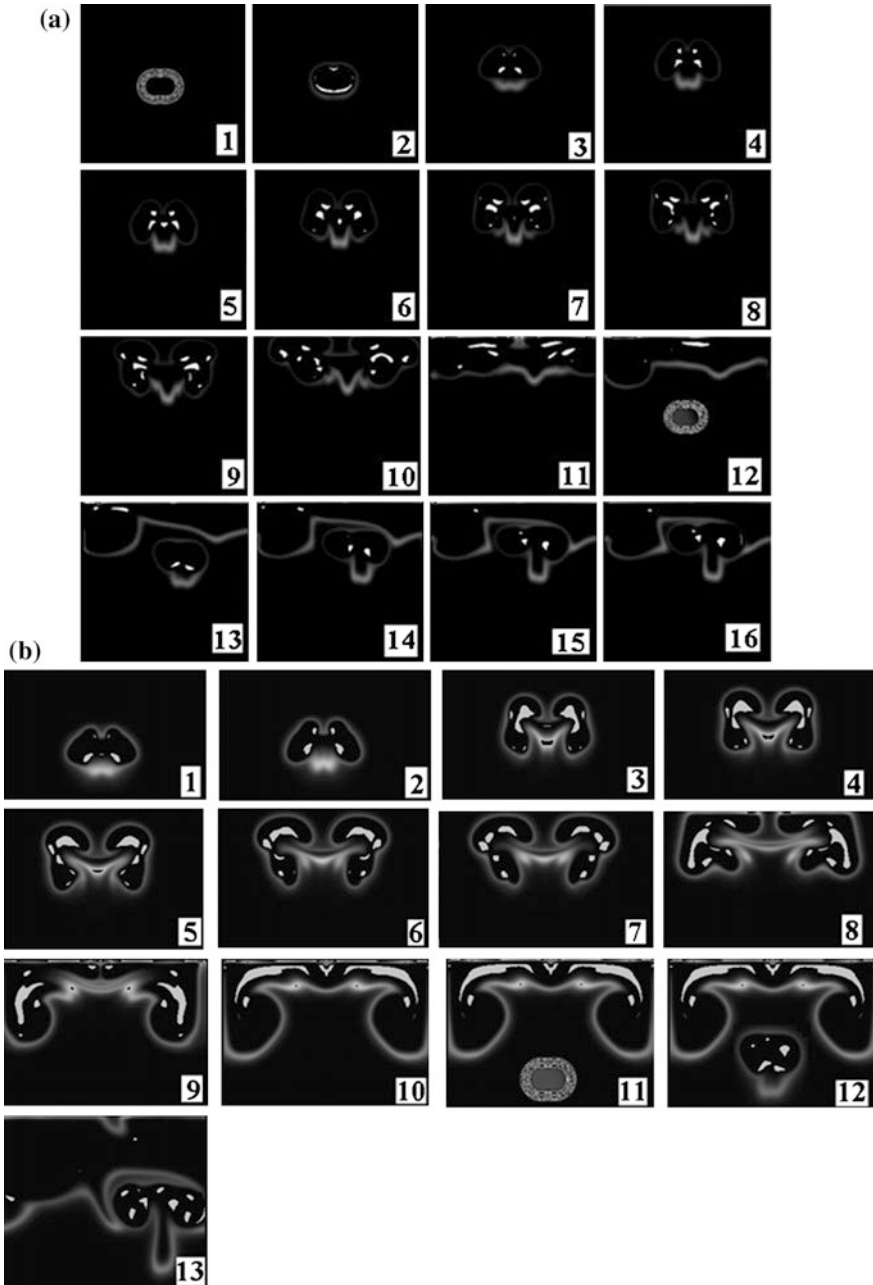


Fig. 2.11 Numerical simulations of the process of cellular FF propagation. **a** 6 % H_2 + 94 % air, $T_o = 298$ K. Time interval between frames 1–11, 12–16 is ~ 0.04 c, between frames 8 and 9 is 0.5 c. **b** 8 % H_2 + 92 % air, $T_o = 298$ K. Time interval between frames 1–10, 11–13 is ~ 0.01 c, between frames 10 and 11 is 0.5 c

used in the present paragraph does not describe the regime of cellular FF propagation in all directions practically with the same velocity (Fig. 2.10c) for $[H_2]_0 > 10\%$, namely the influence of convection is noticeable. The obtained result specifies the limitations of applicability of the Boussinesq approximation for the analysis of flame propagation in lean H_2 –air mixtures as $[H_2]_0$ increases.

As is seen in Fig. 2.11 the calculations performed allowed obtaining qualitative description of both cellular regimes of combustion and increase in cell quantity as $[H_2]_0$ increases for mixtures with $[H_2]_0 < 8\%$. In addition, the possibility is shown of repeated initiation of cellular flame in the mixture, which has already burnt (frame 12 in Fig. 2.11a and frame 11 in Fig. 2.11). This possibility is caused by the movement of both FF and hot reaction products to the top of the reactor. It leads to enrichment of the bottom part of the reactor by H_2 ; therefore, the gas mixture again becomes combustible. The aforesaid is illustrated in Fig. 2.12 in which the calculations of H_2 concentration in the course of cellular FF propagation, corresponding to frames 12–16 in Fig. 2.11a are presented. Notice that the results of calculations are in qualitative agreement with the conclusions of the theory of thermal diffusion instability of flames [1, 38]. So, if all diffusivities are put equal to each other and to thermal diffusivity (thermal diffusion instability is missing), propagation of a smooth flame “upwards” rather than cellular regimes of combustion shown in Fig. 2.11 is observed in calculations.

The influence of the chemical nature of the most quickly diffusing particle on the features of lean H_2 –air flame propagation was investigated numerically. The diffusivity of OH radicals in calculations was put equal to diffusivity of H atoms, and simultaneously the diffusivity of H atoms was put equal to diffusivity of OH radicals, i.e., radicals OH became the most quickly diffusing particle. However, neither

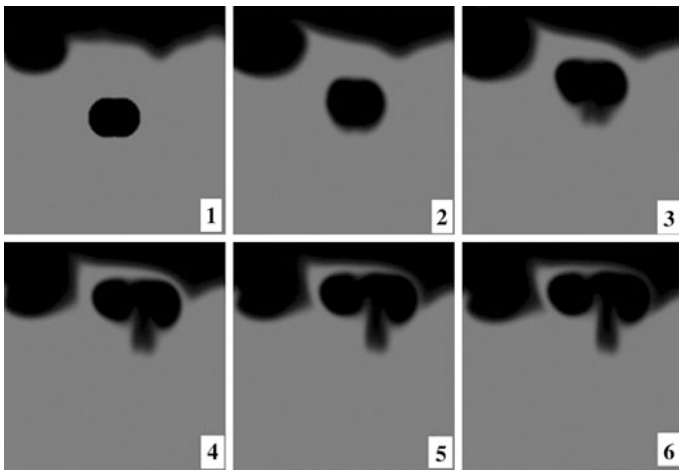


Fig. 2.12 Numerical simulation of H_2 concentration in cellular FF, corresponding to “frames” 12–16 Fig. 2.11b. 6 % H_2 + 94 % air, $T_0 = 298\text{ K}$

cellular character of a flame, nor its velocity considerably changed. It means that within the limitations of calculations performed the regularities of lean hydrogen flames propagation do not depend on the nature of the most quickly diffusing intermediate product, and are determined by the value of diffusivity of the initial insufficient component [1, 38].

References

1. Zel'dovich, Y.B., Barenblatt, G.A., Machviladze, D.V., Teytel'boym, A.A. (ed.): Mathematical theory of flame propagation, 620 pp. Nauka, Moscow (1980) (in Russian)
2. Ksandopulo, G.I., Dubinin, V.V. (ed.): Chemistry of Gaseous Combustion, 240 pp. Chimia, Moscow (1987) (in Russian)
3. Macek, A.: Effect of additives on formation of spherical detonation waves in hydrogen-oxygen-mixtures. *AIAA J.* **1**(8), 1915–1918 (1963)
4. Lewis, B., Von Elbe, G.: Combustion, Explosions and Flame in Gases, p. 566. Academic Press, New York (1987)
5. Zel'dovich, Y.B.: Chain reactions in hot flames—an approximate theory of flame propagation. *Kinet. Catal.* **2**, 305 (1961) (in Russian)
6. Rubtsov, N.M., Seplyarsky, B.S., Tsvetkov, G.I., Chernysh, V.I.: Flame propagation limits in H₂—air mixtures in the presence of small inhibitor additives. *Mendeleev Commun.* **18**, 105–108 (2008)
7. Warnatz, J., Maas, U., Dibble, R.W.: Combustion: Physical and Chemical Fundamentals, Modeling and Simulation, Experiments, Pollutant Formation, 3rd edn, p. 299. Springer, Berlin (2001)
8. Merzhanov, A.G., Haykin, B.I.: Theory of Homogeneous Combustion Waves, 160 p. ISMAN RAS, Chernogolovka (1992) (in Russian)
9. Betev, A.S., Karpov, V.P., Semenov, E.S.: Nonsteady phenomena in propagation of highly curved flames. *Chem. Phys. Rep.* **16**(10), 1861 (1997)
10. Hult, J.: Development of Time Resolved Laser Imaging Techniques for Studies of Turbulent Reacting Flows. *Lund Reports on Combustion Physics*, 120 pp. (2002)
11. Haydon, A.: The Spectroscopy of Flames, 1st edn, 412 pp. Springer, Berlin
12. Rozlovski, A.I. (ed.): Fundamentals of Fire Protection when Operating with Combustible Gases and Vapors, 376 pp. Chimia, Moscow (1987) (in Russian)
13. Seplyarski, B.S., Afanasyev, S.J.: On the theory of hot spot thermal explosion. *Chem. Phys. Rep. (Engl. Transl.)* **17**, 669 (1989)
14. Seplyarski, B.S., Afanasyev, S.J.: Analysis of unsteady explosion of hot spot. *Phys. Combust. Explos.* **22**, 9 (1989) (in Russian)
15. Rubtsov, N.M., Seplyarsky, B.S., Tsvetkov, G.I., Chernysh, V.I.: Influence of inert additives on the time of formation of steady spherical fronts of laminar flames of mixtures of natural gas and isobutylene with oxygen under spark initiation. *Mendeleev Commun.* **19**, 15 (2009)
16. Liu, D., MacFarlane, R.: Laminar burning velocities of H₂—air and H₂—air—steam flames. *Combust. Flame* **49**, 59 (1983)
17. Rubtsov, N.M., Seplyarskii, B.S., Chernysh, I., Tsvetkov, I.: Numerical investigation of the effects of surface recombination and initiation for laminar hydrogen flames at atmospheric pressure. *Mendeleev Commun.* **18**, 220 (2008)
18. Saxena, P., Williams, F.A.: Testing a small detailed chemical-kinetic mechanism for the combustion of hydrogen and carbon monoxide. *Combust. Flame* **145**, 316–323 (2006)
19. Andrae, J., Björnbohm, P.: Wall effects of laminar hydrogen flames over platinum and inert surfaces. *AIChE J.* **46**, 1454 (2000)

20. Aghalayam, P., Bui, P.A., Vlachos, D.G.: The role of radical wall quenching in flame stability and wall flux. *Combust. Theory Model.* **2**, 515 (1998)
21. Azatyan, V.V., Bolodyan, I.A., Navtsenya, V.Y., Shebeko, Y.N.: Dominating role of branching and termination of reaction chains in occurrence of concentration limits of flame propagation. *Russ. J. Chem. Phys. A* **76**, 817 (2002) (2002, 76, 775) (in Russian)
22. Azatyan, V.V., Alexandrov, E.N., Troshin, A.F.: On the rate of chain origination in the reactions of H_2 and D_2 with oxygen. *Kinet. Catal. (Engl.Transl.)* **16**, 346 (1975)
23. Atkinson, R., Baulch, D.L., Cox, R.A., Hampson Jr, R.F., Kerr, J.A., Rossi, M.J., Troe, J.: Evaluated kinetic and photochemical data for atmospheric chemistry: supplement VI. IUPAC subcommittee on gas kinetic data evaluation for atmospheric chemistry. *J. Phys. Chem. Ref. Data* **26**, 1329 (1997)
24. Baulch, D.L., Cobos, C.J., Cox, R.A., Esser, C., Frank, P., Just, Th., Kerr, J.A., Pilling, M.J., Troe, J., Walker, R.W., Warnatz, J.: Evaluated kinetic data for combustion modeling. *J. Phys. Chem. Ref. Data* **21**, 411 (1992)
25. Ryu, S.-O., Hwang, S.M., Rabinowitz, M.J.: Rate coefficient of the OCH via shock-tube laser absorption spectroscopy. *Chem. Phys. Lett.* **242**, 279 (1995)
26. Baulch, D.L., Bowman, C.T., Cobos, C.J., Cox, R.A., Just, Th., Kerr, J.A., Pilling, M.J., Stocker, D., Troe, J., Tsang, W., Walker, R.W., Warnatz, J.: Evaluated kinetic data for combustion modelling: supplement II. *J. Phys. Chem. Ref. Data* **34**, 566 (2005)
27. Yang, H., Gardiner, W.C., Shin, K.S., Fujii, N.: Shock tube study of the rate coefficient of $H + O_2 \rightarrow OH + O$. *Chem. Phys. Lett.* **231**, 449 (1994)
28. Park, Y.K., Vlachos, D.G.: Chemistry reduction and thermokinetic criteria for ignition of hydrogen-air mixtures at high pressures. *J. Chem. Soc., Faraday Trans.* **94**, 735 (1998)
29. Kikoin, I.K. (ed.): *Tables of Physical Values. Handbook*, p. 1007. Atomizdat, Moscow (1976) (in Russian)
30. Hitch, B.D., Senger, D.W.: Reduced H_2 - O_2 mechanisms for use in reacting flow simulation, AIAA-1988-732. In: 26th Aerospace Sciences Meeting, 11 pp. Reno, NV. 11–14 Jan 1988
31. Konnov A.A.: Refinement of the kinetic mechanism of hydrogen combustion. *Chem. Phys. Rep. (Engl.Transl.)* **23**, 10 (2004)
32. Rubtsov, N.M., Kotelkin, V.D., Karpov, V.P.: Transition of flame propagation from a non-thermal mode to a chain-thermal one in chain processes with nonlinear branching. *Kinet. Catal. (Engl.Transl.)* **45**, 11 (2004)
33. Marchuk, G.I.: *Methods of Computational Mathematics*, 608 pp. Nauka, Moscow (1989) (in Russian)
34. Bunev, V.A., Babkin, V.S.: Effect of propylene additives on rich hydrogen-air flames. *Mendelev Commun.* **12**, 120 (2006)
35. Sokolik, A.S. (ed.): *Self-ignition, Flame and Detonation in Gases*. Academy of Sciences USSR, Moscow (1960) (in Russian)
36. Alexandrov, E.N., Kuznetsov, N.M., Kozlov, S.N.: Initiation of chain and thermal explosion with reactor surface. *Phys. Combust. Explos.* **43**, 44 (2007) (in Russian)
37. Williams, F.A., Grcar, J.F.: A hypothetical burning-velocity formula for very lean hydrogen-air mixtures. *Proc. Combust. Inst.* **32**(1), 1351–1360 (2009)
38. Zel'dovich, Y.B.: *Selected Works. Chemical Physics and Hydrodynamics*. Nauka, Moscow (1980) (in Russian)
39. Makarov, D.V., Mol'kov, V.V.: Modeling of dynamics of gas explosion in not ventilated vessel by the method of large whirls. *Phys. Combust. Explos.* **43**, 44 (2007) (in Russian)
40. Ronney, P.D.: Near-limit flame structures at low Lewis number. *Combust. Flame* **82**, 1–14 (1990)
41. Rayleigh, J.W.: On convection currents in a horizontal layer of fluid, when the higher temperature is on the under side. *Philos. Mag.* **32**, 529–546 (1916)
42. Landau, L.D., Lifshitz, E.M.: *Theoretical Physics. Hydrodynamics*, vol. 6. Nauka, Moscow (1986) (in Russian)

43. Chorin, A.J.: A numerical method for solving incompressible viscous flow problems. *J. Comp. Phys.* **2**, 12–26 (1967)
44. Wesseling, P.: An introduction to multigrid methods. Wiley, New York (1992)
45. Samarskii, A.A., Gulin, A.V.: Numerical methods of mathematical physics. Nauchnyi Mir, Moscow (2000) (in Russian)
46. Cashdollar, K.L., Zlochower, I.A., Green, G.M., Thomas, R.A., Hertzberg, M.: Flammability of methane, propane, and hydrogen gases. *J. Loss Prev. Process Ind.* **13**(3–5), 327–340 (2000)



<http://www.springer.com/978-3-319-25932-1>

The Modes of Gaseous Combustion

Rubtsov, N.M.

2016, XXII, 297 p. 127 illus. in color., Hardcover

ISBN: 978-3-319-25932-1